ELSEVIER

Contents lists available at ScienceDirect

Quaternary Science Reviews

journal homepage: www.elsevier.com/locate/guascirev





Holocene humid periods of the Levant – evidence from Dead Sea lake-levels

Yonaton Goldsmith ^{a,*}, Ofer Cohen ^a, Mordechai Stein ^{a,b}, Adi Torfstein ^{a,c}, Yael Kiro ^d, Yochanan Kushnir ^e, Yuval Bartov ^f, Liran Ben-Moshe ^b, Amos Frumkin ^a, Nadav G. Lensky ^{a,b}, Jonathan Keinan ^{a,b}, Lilach Gonen ^a, Yehouda Enzel ^a

- ^a Institute of Earth Sciences, The Hebrew University of Jerusalem, Jerusalem, 91904, Israel
- ^b Geological Survey of Israel, Jerusalem, 91904, Israel
- ^c Interuniversity Institute of Marine Sciences, Eilat, 88103, Israel
- d Department of Earth and Planetary Sciences, Weizmann Institute of Sciences, Rehovot, 76100, Israel
- ^e Lamont-Doherty Earth Observatory of Columbia University, 61 Rt. 9W, Palisades, NY, 10964, USA
- f Mosestro Exploration, Shilat, 7318800, Israel

ARTICLE INFO

Handling editor: P Rioual

Keywords:
Dead sea
Levant
Holocene
Closed-basin lake
Eastern mediterranean
Paleoclimate
Paleohydrology
Archaeology

ABSTRACT

Water availability in the Levant is predicted to decline due to global warming in the upcoming decades and is expected to substantially impact the region. Determining the long-term natural rainfall variability in this region is essential for understanding the regional hydroclimatic response to external climate forcings and for contextualizing future hydroclimate changes. The Dead Sea (DS), located in the southern Levant, is a closed-basin lake whose size varies as a function of water availability. Reconstructing DS lake-level variations through time provides a quantitative measure of the natural hydroclimate variability and can inform on the local hydroclimate response to changes in global climate. Here, we constructed an updated lake-level history of the Holocene DS by: 1) studying lake high-stands derived from a series of new cores collected in the DS southern basin, 2) re-dating of the two major Holocene high-stand exposures, and 3) compiling all previously published ages of Holocene DS lake-level markers (n = 296 radiocarbon ages). The results show that the early (10-6.1 kyr cal BP) and late Holocene (3.6-0 kyr cal BP) in the DS were predominantly wet albeit punctuated by dry intervals, whereas the middle Holocene (6.1-3.6 kyr cal BP) was most likely relatively dry. This pattern of two Holocene humid intervals is also evident in distillation records derived from Levant speleothem caves (which represent the integrated magnitude of rainout from the vapor source to the caves), indicating that rainfall intensity and total water availability were correlated throughout the Holocene. These two humid intervals occurred during high and low summer insolation conditions, suggesting that they were modulated by different climatic mechanisms. The predicted future drying in the Levant is of similar magnitude to the natural hydroclimate variability and thus, it is crucial to assess whether the anthropogenic drying is in- or out-of phase with the natural climate variability.

1. Introduction

The eastern Mediterranean (EM) is considered a climate change "hotspot" where precipitation is predicted to decline by 40% in the upcoming decades, in contrast to the global trend, and is expected to have significant impacts on the region (Hochman et al., 2018). However, the mechanisms responsible for this precipitation decline remain unclear (e.g., Garfinkel et al., 2020; Hochman et al., 2018; Seager et al., 2014; Tuel and Eltahir, 2020). Without a quantitative understanding of the long-term natural rainfall variability in this region and its drivers it is hard to evaluate the severity of future changes, how they compare to the

natural variability, and to identify the potential external forcings that might drive these changes.

The Dead Sea (DS) is an evaporative, hypersaline, closed-basin lake without an outlet, with its size (area and depth) varying as a function of rainfall amount and evaporation (Fig. 1)(Enzel et al., 2003; Morin et al., 2019). In closed-basin lakes, distinct shoreline deposits form at the lake's margin, and serve as physical relict imprints of past lake-levels (Bartov et al., 2002; Bookman et al., 2004; Enzel, 1992; Quade et al., 2018). These shoreline deposits reflect changes in the size of the lake and are therefore, powerful, first order, quantitative recorders of past hydroclimate changes (Benson and Paillet, 1989; Broecker, 2010;

E-mail address: Yonig@mail.huji.ac.il (Y. Goldsmith).

^{*} Corresponding author.

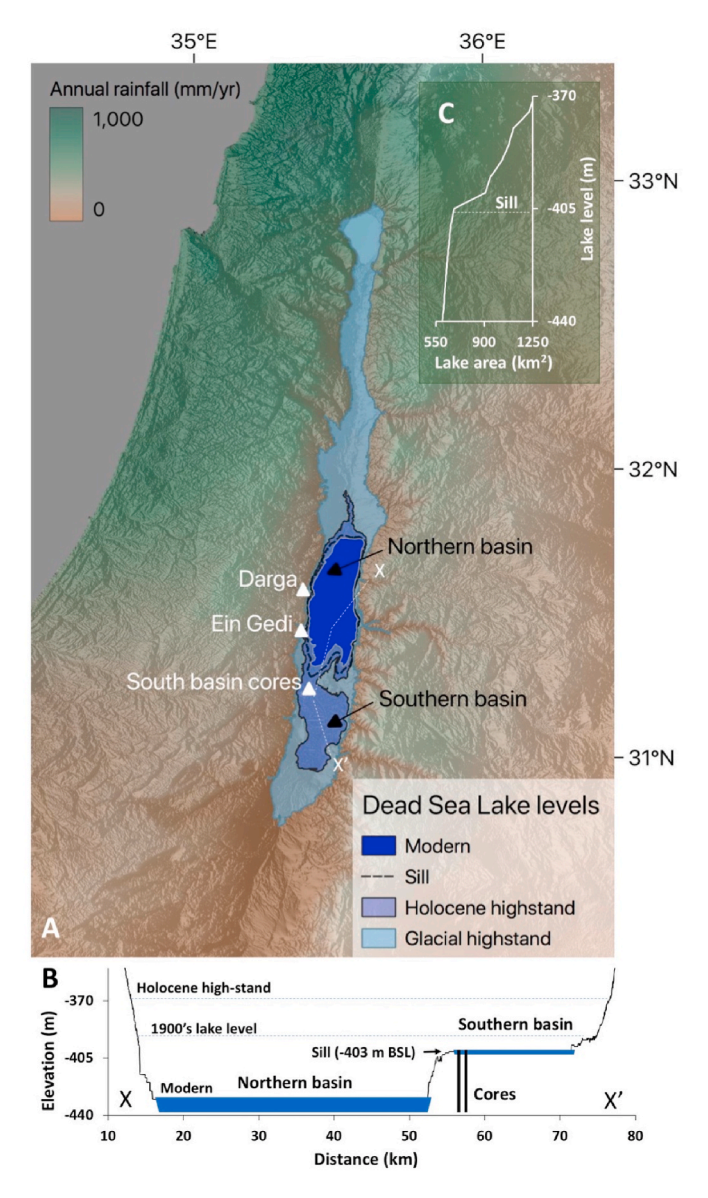


Fig. 1. A. Dead Sea lake-level status superimposed on relief and rainfall maps and showing the location of the two basins, coring site and highstand Holocene outcrops. **B.** A topographic transect through both basins and the coring location. **C.** An hypsometric curve of the DS, showing that changing lake-level below (above) the sill (403 m bsl) results in a small (large) change in surface area.

Broecker and Orr, 1958; Enzel et al., 2015; Goldsmith et al., 2017a, 2022; McGee et al., 2018; Xu et al., 2020). Thus, the DS lake-level history holds valuable information regarding the hydroclimate response of this region to global climate, and provides a quantitative measure of regional natural hydroclimate variability (Bookman et al., 2004; Enzel et al., 2003; Frumkin et al., 2001; Neev and Emery, 1967; Weber et al., 2021).

Over the years, a total of 296 radiocarbon ages were analyzed from Holocene DS lake sediments, which makes the DS sedimentary sequences among the most dated in the world. However, there are still fundamental questions remaining that pertain to the lake-level history of the Holocene DS, and as a result to the regional climate: a) the Holocene lake-level history has been reconstructed in sufficient detail only for the late Holocene (<3.5 kyr cal BP) due to scarce direct lake level markers particularly of early and middle Holocene age, b) there is a general lack of well-dated high-stand deposits, which prevent a full view of the upper bound of the hydrological variability, and c) there is a lack of a

standardized and searchable database of all previous lake-level work and radiometric results, which complicates the ability to compile all previously studied lake-level fluctuations. These gaps prevent: a) a full and better understanding of the long-term hydrological variability in the Levant, and b) evaluating potentially contradicting lake-level markers. In this paper, we aim to reconstruct the high-stands of the Holocene DS and evaluate the natural long-term rainfall variability of this region by: 1) studying lake high-stands derived from a series of new cores collected in the DS southern basin, 2) re-dating of the two major Holocene high-stand exposures, and 3) compiling all previously published ages of Holocene DS lake-level markers.

1.1. Geographical background

The DS is divided into two tectonic basins: a) the northern basin which is ca. 300 m deep and receives runoff from the sub-humid Mediterranean climatic zone at the northern half of the lake's watershed, and b) the southern basin, which is covered today by a shallow salt pan and receives little runoff from the arid southern half of the watershed (Fig. 1). The two basins are separated by a salt diapir located under the Lisan Peninsula, which has been rising since the early Pleistocene (Al-Zoubi and ten Brink, 2001). West of the peninsula, and separated tectonically from the diapir, is a 4 km wide sill (Bartov et al., 2006), today at an elevation of 403 m below sea level (m bsl). The two basins merge into a single water body when the lake-level rises above this sill (Neev and Emery, 1967) (Fig. 1), as was the case during the late 19th and early 20th centuries (Klein and Flohn, 1987). Under such conditions the surface area of the lake is much larger, resulting in enhanced evaporation from the lake. To sustain the lake-level during such times of enhanced evaporation, rainfall must be similarly high. If rainfall is insufficient to sustain such a joint-basins high-stand, the lake will shrink until the lake-level drops below the sill, total evaporation from the lake sharply decreases and a new balance between rainfall and evaporation forms in the northern basin. The southern basin gets cut off from its main water source in the north and progressively dries out. Morin et al. (2019) modeled the sensitivity of the lake-level to hydrological changes above and below the sill. Their results indicate that the lake-level resides below the sill at rainfall amounts of <500 mm/yr (in the northern part of the catchment, that today receive 780 mm/yr), and at these elevations the lake-level is very sensitive to small rainfall changes (2.2 mm/yr per 1 m of lake-level change) (Fig. 1). For the lake to rise above the sill, rainfall amount must exceed 600 mm/yr (in the northern part of the catchment). For the lake to rise from the sill to the level of \sim 385 m bsl, rainfall must reach 1200 mm/yr, at these elevations the surface area is large and thus lake-level is less sensitive to rainfall changes (44 mm/yr per 1 m of lake-level change) (Fig. 1).

During times when the lake-level is below the sill, the southern basin gradually dries out and becomes supersaturated in respect to halite, triggering large halite deposition in the southern basin (Charrach, 2019; Neev and Emery, 1967) (Fig. 2). When the lake-level rises above the sill, relatively "fresher" water from the northern basin overflows into the southern basin and the water there becomes undersaturated to halite, and halite deposition stops. The sediments accumulated in the southern basin during higher-than-sill stands are composed mostly of silty detritus, carried in by the streams and dust (Fig. 2). These silt sediments are most likely also present during low-stands of the lake, but are masked by the large halite deposition. Thus, alternating halite and mud sequences in the southern basin of the DS indicate times when the lake was below and above the sill, respectively, and based on Morin et al. (2019) model these sediments can be used to quantitatively reconstruct distinct wet intervals in the southern Levant.

1.2. Previous reconstructions of Holocene Sead Sea lake-levels

The lake-levels of the DS, and its precursor Lake Lisan, have been studied extensively (Bartov et al., 2002; Bookman et al., 2004; Ebert

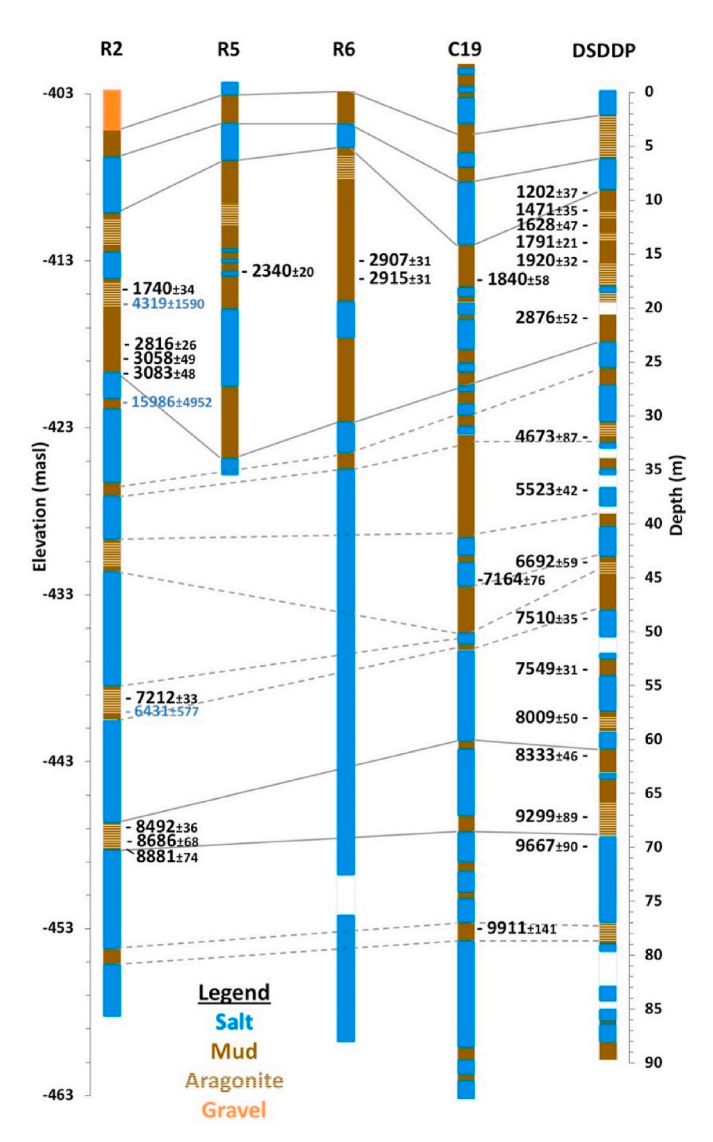


Fig. 2. Core lithology and chronology. Showing the three DSW cores (R2, R5, R6) we studied, the Charrach (2019) composite record of 25 cores from the central southern basin (C19) and the DSDDP lithology (Kiro et al., 2016; Torfstein et al., 2015) and ages (Kitagawa et al., 2017). The cores are composed of halite (blue), silty-clay (brown), aragonite layers (brown with white lines) and anthropogenic gravel at the top (orange). Radiocarbon ages (black), measured on terrestrial macro plant material, are presented as calibrated years before present, U/Th on aragonite layers are in blue. The horizontal solid (dashed) lines denote plausible (possible) correlations between the various cores.

et al., 2021; Enzel et al., 2000, 2003; Frumkin et al., 2001; Kadan, 1997; Kagan et al., 2011, 2015; Langgut et al., 2014; Liu et al., 2013; Migowski et al., 2006; Neumann et al., 2007; Stein et al., 2010; Torfstein et al., 2013a; Weber et al., 2021). The arduous task of constructing a lake-level history, is based on identifying, describing and dating many sediment exposures and cores collected along the lake's margin and compiling the lake-level evidence into a coherent lake-level curve. These studies have shown that Lake Lisan was ~250 m higher than the present lake (and reached ~160 m bsl) during much of Marine Isotope Stages 4-2 (50-20 kyr)(Fig. 1) (Bartov et al., 2002; Torfstein et al., 2013b). During the deglaciation, the lake level dropped to near its pre-industrial elevation (~400 m bsl) (Bartov et al., 2002, 2003; Torfstein et al., 2013b). During the Holocene, the lake fluctuated near its modern levels (370–430 m bsl) (Bookman et al., 2004; Ebert et al., 2021; Enzel et al., 2000, 2003; Frumkin et al., 2001; Kadan, 1997; Kagan et al., 2011; Langgut et al.,

2014; Liu et al., 2013; Migowski et al., 2006; Neumann et al., 2007; Stein et al., 2010; Stern, 2010; Weber et al., 2021; Yechieli et al., 1993). Over the past 60 years, and due to human influence, the lake dropped by ~40 m to its modern elevation of 440 m bsl (e.g., Enzel et al., 2022).

Information on the lake-stands of the DS during the Holocene is derived from three types of sources: exposures of sequences of lake sediments located above the current lake-level, sediments recovered from cores drilled around the lake, and archaeological data. Lake-level data pertaining to the second half of the deglaciation and to the early and middle Holocene (14.6-4 kyr cal BP) are scarce and come mostly from: (a) cores along the margins of the lake, which only provide an estimates of minimum lake-level (Migowski et al., 2006; Stein et al., 2010) and (b) two exposures of high-stand lake sediments in Nahal Darga (Enzel et al., 2000; Kadan, 1997; Liu et al., 2013) and Ein Gedi (Bartov, 2004; Weber et al., 2021). However, some of the pre- 6.5 kyr cal BP chronology is based on bulk sedimentary organics, which may be prone to large reservoir effects (Enzel et al., 2000; Kadan, 1997). Late Holocene highstand outcrops have been reported in Nahal Ze'elim and Nahal David (Bookman et al., 2004), and Mt. Sedom (Frumkin et al., 2001) and its surroundings (Migowski et al., 2006). Mt. Sedom is an active salt diapir that has been rising at a rate of 5-10.5 mm/year (Frumkin et al., 2001; Weinberger et al., 2006), and thus, it is complicated to extract the exact lake-level represented by samples collected on or adjacent to Mt. Sedom. Additional information on late Holocene highstands comes from two sources: a) archaeological remains of two sites dated to the 1st millennia BCE (Rujm el-Baher and Khirbet Mazin, at an elevation of 393 m bsl, Hirschfeld, 2006) that served as small anchorage ports of the DS, and b) historical elevation data from the 19th century CE (e.g., Klein and Flohn, 1987).

Part of the Holocene highstand data come from cores drilled in the southern basin of the DS, which contain alternating halite and silty-clay deposits (Charrach, 2019; Neev and Emery, 1967)(Fig. 1). Neev and Emery (1967) dated aragonite layers and bulk organic material from lake sediments, which are both potentially affected by an unknown reservoir effect, rendering their results questionable. Charrach (2019) found and successfully dated plant remains from three of these layers, and thus currently, most of the silty-clay layers have not been dated and the timing of most of these deposits and the flooding of the southern basin remain unclear.

To provide a fuller and updated perspective on the Holocene high-stands of the DS, we present in this paper: 1) A new record of Holocene DS high-stands, derived from three cores collected in the southern basin of the Dead Sea, which represent times when the lake level rose above the sill and filled the southern basin. 2) A detailed reconstruction and re-dating of sediments associated with the two major Holocene high-stand of the DS at Nahal Darga and Ein Gedi. 3) A comprehensive database of 296 radiocarbon ages of all previously dated Holocene lake status records. This compilation enables, for the first time, a comparative evaluation of all previous Dead Sea research pertaining to its Holocene level reconstruction and portrays a full framework of what is known about the Holocene lake level after decades of research, and what information is still missing.

2. Methodology

2.1. Analyzing the southern basin cores

During 2021, the Dead Sea Works (DSW), the Potash extraction company, drilled a series of cores into the northern tip of the southern basin for geotechnical purposes (Fig. 1, Fig. S1). We were granted permission to study these cores, once the geotechnical analysis was completed. The cores, characterized by the DSW, are 20–60 m in length and contain predominantly massive halite deposits (Fig. 2). In nine intervals, mud layers (ranging in thickness between 10 and 200 cm) are present. As explained above, we interpret these mud layers as representing times when the lake-level rose above the sill and indicate wetter

conditions in the southern Levant. The cores, post geotechnical sampling, were fragmented and discontinuous and some parts of the cores were not well preserved. We focused our sampling efforts on pristine intervals, where the original sedimentary structure was maintained (Fig. S1).

2.1.1. Radiocarbon ages

From the intact sections in three of the cores, we sieved the mud layers and picked out 11 samples of macro-plant material and charcoal. Not all mud layers contained macro-plants. Therefore, to evaluate whether it is possible to date these layers using bulk sedimentary radiocarbon, we also sampled and measured two bulk organic samples adjacent to macro-plant samples. This test will also enable us to assess the reliability of the Neev and Emery (1967) data, who used bulk sample radiocarbon ages from their southern basin cores. Radiocarbon measurements were conducted at The Keck AMS laboratory at University of California Irvine, California. The results are presented as calibrated years before present (yr cal BP) and the presented uncertainty is 1σ (Table S1).

2.1.2. Finger-printing the water source of the southern basin using aragonites U-Th

We interpret the mud layers in the southern basin cores as representing times when the DS rose above the sill and water from the northern basin flowed into the south basin. An alternative source of this water could be river inflow into the south basin from the southern part of catchment. To fingerprint the water source, we used U isotopes in the fine aragonite layers present in some of the mud layers from the southern basin (Fig. 2, Fig. S1). Similar aragonite layers have been identified in the northern basin, and termed "laminated detritus" (ld) layers and have been studied in great detail (Bookman et al., 2004; Haliva-Cohen et al., 2012). U isotopes in these aragonite layers have been proposed as tracers of the water source that filled the lake. Kiro et al. (2020) showed that northern and southern water sources entering the DS have substantially different U-isotope ratios, which are recorded in the aragonite layers and can serve as a water source tracer. Thus, U-isotopes can distinguish between two potential water sources that could have filled the southern basin: 1) water overflowing the sill from the northern basin, and 2) water flowing in from the Arava River in the south; this does not require a flooding of the sill and could occur also during lower lake-stands.

In addition, U–Th disequilibrium dating of the DS aragonite laminae was attempted based on previous successes (e.g. Haase-Schramm et al., 2004; Torfstein et al., 2013a). The DS aragonites are characterized as "dirty carbonates" containing initial ²³⁰Th derived from two sources: detrital sedimentary Th and hydrogenous Th, where the former is thought to introduce a much larger error than the latter for young samples (Haase-Schramm et al., 2004). To correct for these two sources of uncertainty, we used two approaches: 1) a single sample correction method, which uses previously established initial detrital Th $(^{232}\text{Th}/^{238}\text{U}~=~0.85)$ and hydrogenous Th (Th =~0.08 ppm and 232 Th/ 230 Th = 44,000 atomic) values (Haase-Schramm et al., 2004; Torfstein et al., 2013a), and 2) an Osmond-type isochron method (Ludwig, 2003), where the initial 230 Th/ 238 U is calculated as the intercept of a^{232} Th/ 238 U vs. 230 Th/ 238 U isochron diagram (Fig. S2). To account for uncertainty in the detrital end-member, we varied the Th/U detrital end-member (0.85, 1, 1.25 and 4, and assigned an error of 10% for each value), and assumed the detrital end-member is at secular equilibrium and thus provides the detrital ²³⁰Th/²³²Th (See Torfstein et al., 2013a for detailed methods).

We sampled three aragonite layers, of which two were adjacent to macro-plant material that were also radiocarbon dated. From within these layers, we sub-sampled two or three individual samples and analyzed their chemistry using an ICP-MS and their U-Th isotopes using a Neptune Plus MC-ICP-MS, both at the Hebrew University. Chemical, analytical and data-reduction procedures follow Torfstein et al. (2013a,

2015).

2.1.3. Assigning a lake-level to the mud layers of the southern basin cores. As discussed above, we interpret the mud layers as times when the lake rose above the sill (an assumption that we test using U isotopes, see above). However, the evolution of the sills' elevation is unclear. The early lake-level reconstructions assumed that sill remained at an elevation of 403 m bsl throughout the Holocene (e.g., Bookman et al., 2004; Migowski et al., 2006). Though, Charrach (2019) calculated the sill's elevation based on sedimentation rate and accommodation space, and concluded that the sill was at 420 m bsl in the early Holocene and rose to 403 m bsl throughout the Holocene due to sediment accumulation. Therefore, when assigning the minimum lake-level elevation at the time of the mud deposition, we present two scenarios: a) the sill was at 403 m bsl throughout the Holocene, and b) the sill rose from 420 m bsl in the early Holocene to 403 m bsl in the late Holocene (black and red dashed lines in Fig. 3, respectively).

2.2. Reevaluating Holocene high-stands from the Darga and Ein Gedi exposures

The highest Holocene lake sediment outcrops in the DS have been described and dated in Nahal Darga (Enzel et al., 2000; Kadan, 1997; Liu et al., 2013) and Ein Gedi (Bartov, 2004; Weber et al., 2021) (Figs. 1 and 3, S3 and S4). As described above, there are missing or contradicting elevation data from these sections, questioning the reliability of the ages and some debate over the geomorphological interpretation of these sections. We returned to these two sites and resampled the sections. Elevation of the samples was determined using data from an airborne light detection and ranging system (LiDAR) courtesy of the Geological Survey of Israel (e.g., Enzel et al., 2022), which provides centimeter-scale resolution. Charcoal, macro-plants and freshwater snails were sampled from within these sections. Radiocarbon measurements on these samples were conducted at The Keck AMS laboratory at University of California Irvine, CA.

2.3. Constructing a Holocene Dead Sea lake-level database

Over the past 50 years, over a dozen papers have dated Holocene stratigraphic sections in the DS basin, which combined include 296 radiocarbon ages (Bookman et al., 2004; Ebert et al., 2021; Enzel et al., 2000, 2003; Frumkin et al., 2001; Kadan, 1997; Kagan et al., 2011; Langgut et al., 2014; Liu et al., 2013; Migowski et al., 2006; Neumann et al., 2007; Stein et al., 2010; Stern, 2010; Weber et al., 2021; Yechieli et al., 1993). We constructed an online database that contains all the radiocarbon samples and includes: metadata (author names, journal, etc.), location coordinates, sample elevation, sediment characteristics, sample material, dating lab, and original interpretation of lake-level status by the original authors (Table S6). For a few of the earlier works done on the DS, not all elevation data exists in the original publications (Bartov, 2004; Enzel et al., 2000; Frumkin et al., 2001; Kadan, 1997; Liu et al., 2013; Migowski et al., 2006). In such cases, we either returned to the sites and measured the elevation with a GPS, or used the LiDAR elevation data to assign the correct height. The reevaluated elevations are noted in the database.

All radiocarbon samples were calibrated individually using Intcal20 in the Oxcal program (Reimer et al., 2020). Some of the samples come from sedimentary sequences that contain a few sedimentary units and have a series of ages and replicate samples, some sections have reported hiatuses and some have undated beach ridges. For these sedimentary sequences, we tried using the "sequence" option in Oxcal, which estimates the ages and age range of unknown stratigraphic boundaries (in this case, either hiatuses or beach-ridges) using the age-depth model and sedimentation rate (Ramsey, 2008). Due to the large uncertainty involved in such interpolation of the data, this method results in large dating uncertainties (~hundreds of years, which is too large for our

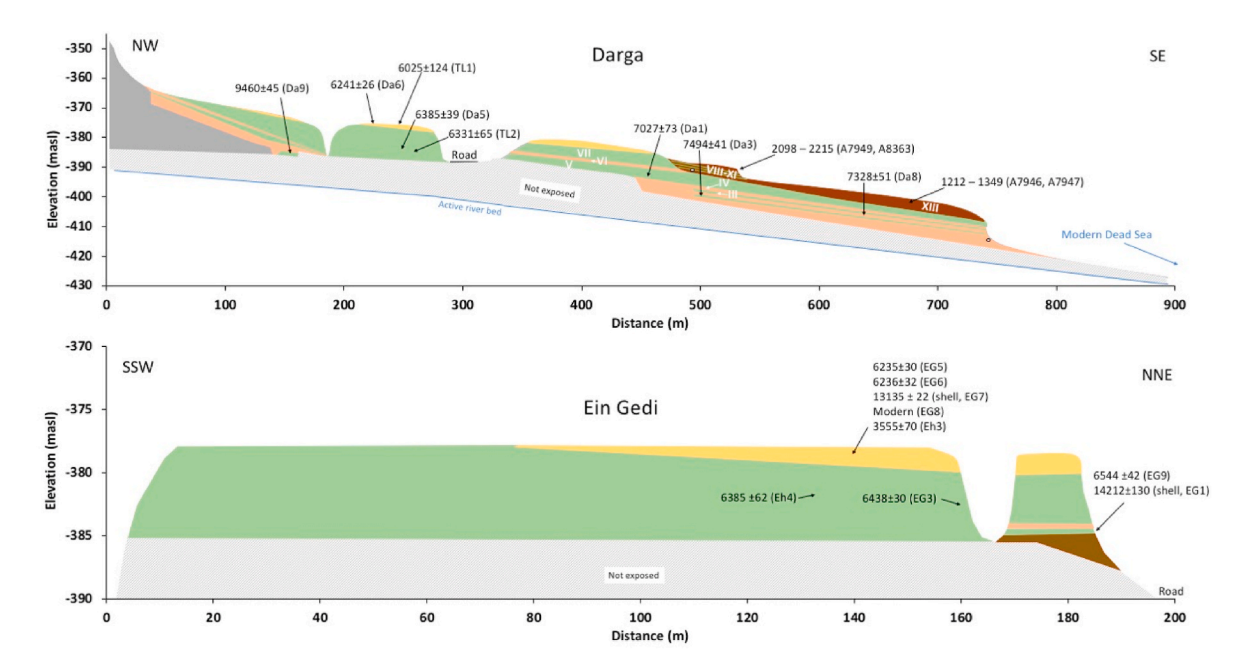


Fig. 3. Sedimentary sections of Darga (top) and Ein Gedi (bottom). Darga: The base of the section is composed of sediments of an unknown age (gray), above this unit, on an angular unconformity, are middle Holocene (7.5–6.3 kyr cal BP) thick brown laminated lake sediments (green), with syndepositional beach-ridges (orange) and capped by a middle Holocene (6.2–6.0 kyr cal BP) beach-ridge (yellow). Above the middle Holocene sequence in an angular unconformity with late Holocene beach-ridges (brown) and syndepositional lake sediments (light green) (2.2–1.2 kyr cal BP). Road and bridge landfill sediments and talus (hatched gray lines) extend from the exposure to the active river bed (blue) and obscure the stratigraphy. Original units defined by Kadan (1997) (white roman numerals) and calibrated (yr cal BP) radiocarbon ages (black) from Kadan (1997, A#, where # stands for the sample number), Liu et al. (2013, TL#) and this study (Da#). Units that have more the one sample dated are shown as the calibrated range of the samples (e.g., the younger Darga units). There are two pipes that stick out of the section (black-white circles), these are drawn as geographical markers. Ein Gedi: The base of the section is composed of alluvial gravel (dark orange), above there is a lacustrine unit (green) with a syndepositional alluvial deposit (orange). Above are middle Holocene (6.4–6.3 kyr cal BP) thick brown laminated lake sediments (green). The section is capped by a middle Holocene (6.2 kyr cal BP) beach-ridge (yellow). At the base of the section there is a talus which obscures the lower part of the stratigraphy (hatched gray lines). Calibrated (cal BP) radiocarbon ages (black) are from Bartov (2004, Ehx) and this study (EGx). There are 5 ages from the upper beach-ridge, 2 are from charcoal, one is from a modern chard root and from a melanopsins shell. Bartov's (2004) age from the beach-ridge (3.6 kyr cal BP) is an outlier, and could be a mixture of the charcoal (6.2 kyr cal BP) and chard root (modern).

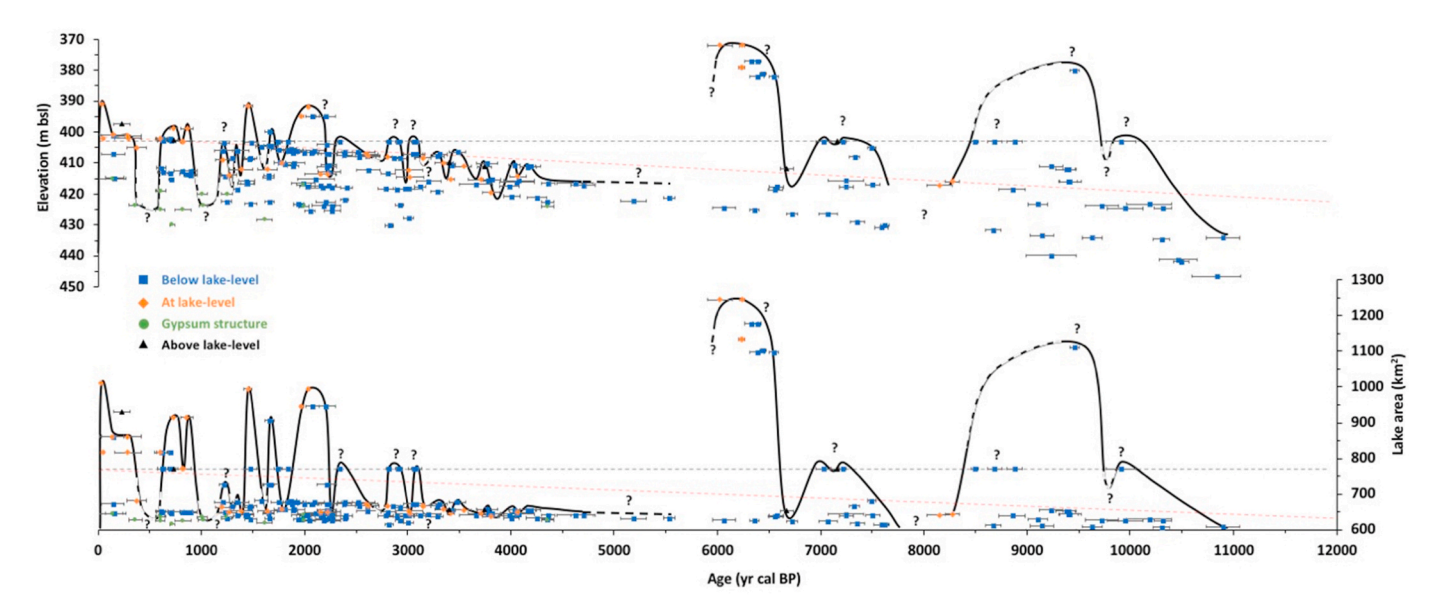


Fig. 4. Dead Sea lake-level (top) and lake area (bottom). Dead Sea lake-level indicators (blue square – below lake-level, orange diamond – at lake-level, black triangle – above lake-level, green circle – gypsum structure) and interpreted lake-level (solid black line for places where the lake-level is well constrained, dashed lines for places where the lake level is less certain). Question marks indicate places where the direction of the lake-level is known but the magnitude is not. All samples are presented as the mean of the Intcal20 calibrated radiocarbon ages, and the uncertainty is 1σ (Fig. S5 shows the same data with a 2σ uncertainty). The figure presents the 238 ages that fit the criteria presented in the text (e.g. are not outliers, on organic material or come from uplifted regions, for all data see Fig. S5). The elevation or area of the sill are marked by horizontal dashed lines (black line represents the scenario where the sill elevation remained constant and the red line represents the Charrach (2019) scenario where the sill rose 17 m throughout the Holocene).

assessment). As there are many directly dated samples that are much better constrained than the interpolated data, we use the interpolated ages only as supplemental indicators for the lake-level reconstruction and not as standalone data (see full data in Fig. S5a). Both the single sample and sequence results are presented in Table S6.

All calibrated data were plotted using the original interpretation of the lake-level status (Fig. S3). These include: sedimentary markers deposited at, or very near, the shore of the lake (e.g., beach ridges and shoreline deposits), sedimentary indicators of minimum lake-level (e.g., silty lacustrine sediments that were deposited below the water level), and indicators of upper boundary lake-level (e.g., gravels that were deposited in an alluvial setting outside of the lake) (Fig. S5). Gypsum structures have been interpreted as near shore deposits where saline springs and the DS brine mix causing gypsum deposition (Weber et al., 2021). However, as they are not "classic" shoreline sediments, we categorized them separately.

Once all dated samples and modeled beach-ridges and hiatuses were plotted as a function of their age, age uncertainty and height, it was possible to construct a new lake-level curve (Fig. 4). The presented lake-level curve is one possible, but the most reasonable, interpretation of the data and was constructed to account for as many data points as possible, within their prescribed 1σ age uncertainty. In places where there are clear lake-level markers (beach ridges, archaeological remains, etc.), a solid line is drawn. In places where there are insufficient data (e.g., between 4.5 and 5.5 kyr cal BP) a dashed line was drawn. A question mark denotes places where the direction of the lake-level change is clear but not its exact elevation. In places where there are gaps in the data, or if the extent of the high or low stands are unknown, a question mark is added.

3. Results

3.1. The cores from the Dead Sea southern basin

3.1.1. Core lithology

The three analyzed cores, R2, R5, and R6 (Fig. 2), present quite similar lithological sequences. The upper 20 m of each core are composed predominantly of silty-clay sediments. Below this depth, the cores are composed primarily of halite with a few thin layers of silty-clay sediments.

R2, the most southern core, and the most intact one, is $59.5 \,\mathrm{m}$ long. It is predominantly composed of nine layers of halite with a total thickness of 34 m alternating with nine layers of silty-clay sediments with a total thickness of 19 m. These silty sediments were examined for plant remains; eight of them contained sufficient material for radiocarbon analyses. Three aragonite layers were selected for U/Th dating (Fig. 2 and S1).

Core R5 is a 26 m long core, half of this length is composed of silty-clay sediments (in four layers and a total of 13 m of silty-clay sediments) and the other half is composed of halite (four halite layers, where one salt layer has three sub-layers, and a total of 11 m of halite) (Fig. 2 and S1). Previous sampling by the DSW left this core very fragmented and the only remaining undisturbed silty-clay sediments layer is at a depth of 10-12 m; two samples from this silty-clay sediment layer were collected for radiocarbon analyses.

Core R6 is a 60 m long core predominantly composed of five layers of halite with a total thickness of 41 m, alternating with six layers of silty-clay sediments with a total thickness of 17 m (Fig. 2 and S1). Previous sampling by DSW left this core very fragmented and the only remaining undisturbed silty-clay sediment layer is from a depth of 9–11 m; two samples from this silty-clay sediment layer were collected for radio-carbon analyses.

The silty-clay sediments occasionally contain finely laminated aragonite, (Ben Dor et al., 2019; Bookman et al., 2004; Haliva-Cohen et al., 2012) (Fig. S1). Such aragonite laminae have been interpreted as indicators of times with relatively high inputs of fresh water into the

lake, which supply the HCO₃⁻ required for aragonite precipitation (Ben Dor et al., 2019; Bookman et al., 2004; Stein et al., 1997).

3.1.2. Radiocarbon ages of mud layers in the southern basin cores

The radiocarbon analysis results show that the 60-m long sequences in the core date back to ~ 9 cal kyr BP, i.e., they cover much of the Holocene (Fig. 2 and Fig. S1). The radiocarbon ages show a systematic increasing trend of ages with depth. The three cores show similar ages at similar depths. The calibrated ages for the silty-clay sediment layers are: 8.9–8.5, 7.2 and 3.1–1.7 cal kyr BP.

The paired plant material and bulk sediment radiocarbon ages show a 2500-year difference (Table S1). This indicates that the DS southern basin has a significant reservoir correction age. Neev and Emery (1967) dated bulk sediments radiocarbon from a series of cores from the southern basin. Our results indicate that their results were most likely too old and should be reevaluated.

3.1.3. Fingerprinting the source of water in the southern basin using U/Th ²³⁴U/²³⁸U activity ratios are used to fingerprint the water sources to the lake (Kiro et al., 2020). Initial ²³⁴U/²³⁸U values of the aragonites, calculated using the isochron method and for different detrital end member Th/U ratios, range between 1.38 and 1.46 (Fig. S2, Table S4 and see Supplementary Text for additional results of the aragonite chemistry). The single sample correction method yielded $^{234}\text{U}/^{238}\text{U}$ activity ratios between 1.28 and 1.39. The 234U/238U activity ratios of southern basin aragonite are similar to those measured in DS waters sampled in 1978 CE (1.44, Haase-Schramm et al., 2004), waters from the western DS catchment (>1.43, Kiro et al., 2020), and aragonites from the Holocene DSDDP (1.34-1.43, Torfstein et al., 2015). They are also similar to 234 U/ 238 U activity ratios of the MIS 6 and MIS 5d-5a DS aragonites (1.34-1.54, Kiro et al., 2020) and are slightly lower than the values of the Lisan (1.47–1.54, Haase-Schramm et al., 2004). In contrast, the ²³⁴U/²³⁸U activity ratios of the Holocene aragonites recovered from the southern basin are significantly higher than the ²³⁴U/²³⁸U activity ratios of the waters reaching the lake by its eastern and southern catchments (1.1-1.2, Kiro et al., 2020). These results indicate that the source of the water that filled the southern basin of the DS is most likely overflow from the northern basin and not the southern and eastern watershed of the lake. i.e., they indicate the formation of a connected single lake covering both basins.

U–Th ages of three dirty aragonite samples were calculated using the isochron method (Supplementary Text, Tables S3 and S4 and Fig. S2). Two of the isochron ages (from depths of 11.14 m and 36.2 m) are identical, within the age uncertainty, to the radiocarbon ages (Fig. 2 and Fig. S1). The third sample (from a depth of 23.0 m) is very different from the radiocarbon ages above and below it, regardless of the ascribed detrital end-member composition. As the U–Th dating of the samples from the core yielded much larger uncertainties than the radiocarbon ages, we rely exclusively on the radiocarbon chronology.

3.1.4. Assigning a lake-level to the mud layers from the southern basin cores

The two scenarios of constant sill elevation vs. a ~20 m rise of the sill
throughout the Holocene, result in very similar lake-level curves that do
not change the lake-level or the lake-area reconstructions (black and red
dashed lines in Fig. 3, respectively), and thus, we use the constant sill
elevation for the rest of the this paper. However, the elevation assignment of the southern basin mud layers should be reevaluated once a
more thorough research into the evolution of the sill is conducted.

3.2. Re-dating high Holocene lake stands

The elevation of the Ein Gedi section is 386 to 379 m bsl (Fig. 3, Fig. S4). The base of the section is composed of two alluvial units (total 3 m thick) separated by a thin, fine-grained lacustrine sediment containing freshwater snails. This basal unit is overlain by a 4-m thick white-reddish laminated silty lacustrine sediments, dated by Bartov (2004)

to 6385 \pm 62 cal yr BP. We sampled additional charcoal from a sandy layer located 2 m above the base of this laminated lacustrine unit. This sample yielded an age of 6437 \pm 30 cal yr BP (EG3), very similar to Bartov's age (Table S2). An erosional unconformity marks the top of the laminated lacustrine unit. The unconformity is capped by a well-sorted beach ridge deposit associated in the field with finely laminated silty lagoonal sediments that accumulated landward of the beach ridge. These lagoonal sediments contain charcoal and freshwater snails deposits, dated by Bartov (2004) to 3555 \pm 70 cal yr BP. Because of its importance as a marker of a high stand of the lake, this layer has been the subject to some debate. Therefore, we resampled three different components of these lagoonal sediments: two charcoal samples, one twig/root (suspected already during sampling in the field as possibly modern), and a freshwater gastropod. The freshwater gastropod (Melanopsis sp.) originated from springs at the margin of the lake, and most likely indicate times of increased spring discharge into the lake. The charcoal samples returned ages of 6235 \pm 30, 6236 \pm 32 cal yr BP, the twig/root was dated as modern, and the shell dated to 13,125 \pm 22 cal yr BP (EG5,6,8,7, respectively) (Table S2). These ages differ substantially from that of Bartov (2004), and as we could not reproduce this age, we do not consider it in the following discussion. Below the laminated lacustrine unit there is a layer of gravel, and underlying it is a 30 cm thick fine-grained lake sediment, with lacustrine gastropods. We dated charcoal and a gastropod that yielded ages of 6544 \pm 42 (EG9) and 14, 212 ± 130 (EG1) cal yr BP, respectively.

The elevation of the Darga exposure spans from 407 to 372 m bsl, and is divided into the eastern and western exposures by the main DS highway (Fig. 3, Fig. S3). East of the highway and the lower part of the outcrop has been only recently exposed due to continuous channel incision. It was not visible in the mid-1990s when Enzel et al. (2000) and Kadan (1997) documented this exposure. The base of the section comprises three alluvium layers (~4 m thick in total) that are separated by two thin, fine-grained lacustrine beds that contain charcoal and freshwater snails. The charcoal yielded ages of 7494 \pm 41 cal yrs BP (Da3) and 7328 \pm 51 Cal yrs BP (Da8)(Table S2). Above this layer, there are 6 m of laminated white-reddish clay-silt lake sediments, that rise progressively westward, where they reach an elevation of 372 m bsl. This unit was dated by Kadan (1997) to 9.2-7.7 kyr cal BP using sedimentary organic material [units 3-7 in Kadan's (1997) work]. We collected a charcoal sample from the base of the lacustrine sediment, a few centimeters above the contact with the lower alluvial layer (403 m bsl), which yielded an age of 6995 \pm 73 cal yr BP (Da1). This age is somewhat younger than what was reported by Kadan (1997) indicating that sedimentary organic material in the northern basin of the DS has a large reservoir effect, similar to what we find in the southern basin.

West of the highway, the base of the western outcrop comprises small (2m × 2m) lacustrine sediment patches that are truncated by an erosional unconformity (Fig. 3). Charcoal from these lacustrine sediments yielded and age of 9460 \pm 45 cal yr BP (Da9). These lacustrine sediments are currently the only high-stand exposure from the early Holocene in the DS basin. Above this unconformity is a 6 m thick lacustrine layer that continues into the eastern exposure, where its base was dated (Da1). We dated charcoal material collected 3 m below its top (377 m bsl), a sample yielded an age of 6394 \pm 39 cal yr BP (Da5). This age is identical to the age reported by Liu et al. (2013) from the same location and to the ages of the lacustrine unit in the Ein Gedi outcrop (reported above). This Darga lacustrine unit is truncated by an erosional unconformity and is capped by a beach ridge (at 372 m bsl), which was dated by Liu et al. (2013) to 6025 \pm 124 cal yr BP. A charcoal sample we collected from this beach ridge yielded an age of 6241 \pm 26 cal yr BP (Da6), which is very similar to both Liu et al. (2013) age, and to the age of the beach ridge that caps the Ein Gedi outcrop (Table S2).

3.3. Dead Sea lake-level compilation

The compilation contains 296 radiocarbon ages described in 19

papers and MSc and PhD theses (Fig. 4, Fig. S5 and Table S6). Of these, samples designated as outliers by the original authors (n = 9), dated by bulk organics (n = 9) or older than 12 kyr cal BP (n = 11) and snail samples with a very large reservoirs effect (n = 2) were not used in our lake-level reconstruction. The data derived from the uplifted caves at Mt. Sedom (Frumkin et al., 2001) are not used for the lake-level reconstruction (n = 25), but were previously applied to calculate the uplift rate of Mt. Sedom diapir and constrain the uplift of the late Holocene shoreline at Arubotaim Cave (Frumkin et al., 2001) (Fig. S5 and supplementary text). The final lake-level was reconstructed based on the remaining 238 ages. Of these, 45 are dated beach ridges or samples from near-shore environments, six are from alluvial units, 166 are from lacustrine sediments, and 21 samples are from gypsum structures (Fig. 4). The compilation of all existing lake-level data show that throughout the Holocene, the DS lake-level fluctuated ~68 m (from 440 to 372 m bsl). In Fig. 4, we present the data using the 1σ error of the calibrated ages. The relatively small errors, force, in some places, the lake-level to vary rapidly. Using a 2σ error reduces some of these rapid fluctuations, we present both records for comparison in the supplementary material (Fig. S5).

4. Discussion

4.1. The Holocene lake-level history of the Dead Sea

The compiled lake-level chronology, derived from the 238 radio-carbon ages from lake-margin exposures, southern basin cores, and from shallow cores from the western margin of the DS, provides a detailed history of the hydrological mass balance of the DS watershed and is the most direct and updated hydrological history of the Levant throughout the Holocene (Fig. 4). Additional important information regarding the DS lake status are derived from the deep core drilled into the depocenter of the northern basin and its lithological and geochemical proxies retrieved by the Dead Sea Deep Drilling Project (DSDDP) (Goldstein et al., 2020; Kiro et al., 2020; Kitagawa et al., 2017; Neugebauer et al., 2014; Torfstein et al., 2015). Below, we combine these two sets of records, the levels from the margins and inferences from the core, and provide a hydrological and limnological history of the Holocene DS and discuss its implications.

The early Holocene was characterized by large lake-level fluctuations, where the lake rose and fell substantially (levels ranged from 372 to 420 m bsl). There are two intervals where the lake reached its highest point (9.5 and 6.5-6.1 kyr cal BP). During two additional high-stands (9.9 and 7.5-7.0 kyr cal BP) the lake rose above the sill; the maximum levels associated with them remain unclear. These four high lake-level intervals are evident by four mud deposits in the southern basin, three of which were dated directly from the cores (at depths: 455, 447, 439 mbsl in core R2, Fig. 2), and the youngest, undated mud layer (at a depth of 430 mbsl in core R2, Fig. 2) is most-likely correlated with the dated high-stand sediments in Ein Gedi and Darga (at \sim 375 m bsl). Near-shore deposits at an elevation of ~415 m bsl at 8.1 and 6.7 kyr cal BP indicate that the lake level dropped substantially between these wet phases (Migowski et al., 2006; Neumann et al., 2007, respectively). The reconstructed lake level fluctuations between wet and dry intervals are clearly reflected by silt and halite deposits in the both the DSDDP core and the southern basin cores.

It seems that deposits associated with the 9.5 kyr cal BP high stand have been almost entirely eroded away by the subsequent 6.5 kyr cal BP transgression, which is the highest documented highstand of the entire Holocene at 372 m bsl. Such deposits were, thus far, observed only at one patchy exposure in Darga. It is plausible that additional intervals of high lake-level occurred during the Early Holocene (recorded by mud deposits in the south basin), but evidence for them has been eroded or yet to be recognized. This limits the ability to robustly reconstruct the Early Holocene size of the lake. We reconstructed high lake-levels between 9.5 and 8.3 kyr cal BP by tying together three observations: 1) the

9.5 kyr cal BP high-stand, 2) the 8.9–8.5 kyr cal BP mud deposits in the southern basin indicating that the lake level was above the sill, and 3) the lithology of the DSDDP shows a continuous deposition of aragonite and mud in the depocenter of the lake between 9.6 and 8.3 kyr cal BPs,

most probably indicating a prolonged wet interval.

At 6.1 kyr cal BP, the lake-level dropped substantially. Since this time, the lake has most likely not exceeded an elevation of 390 m bsl. This large lake-level drop is coeval with the proposed demise of Sapropel

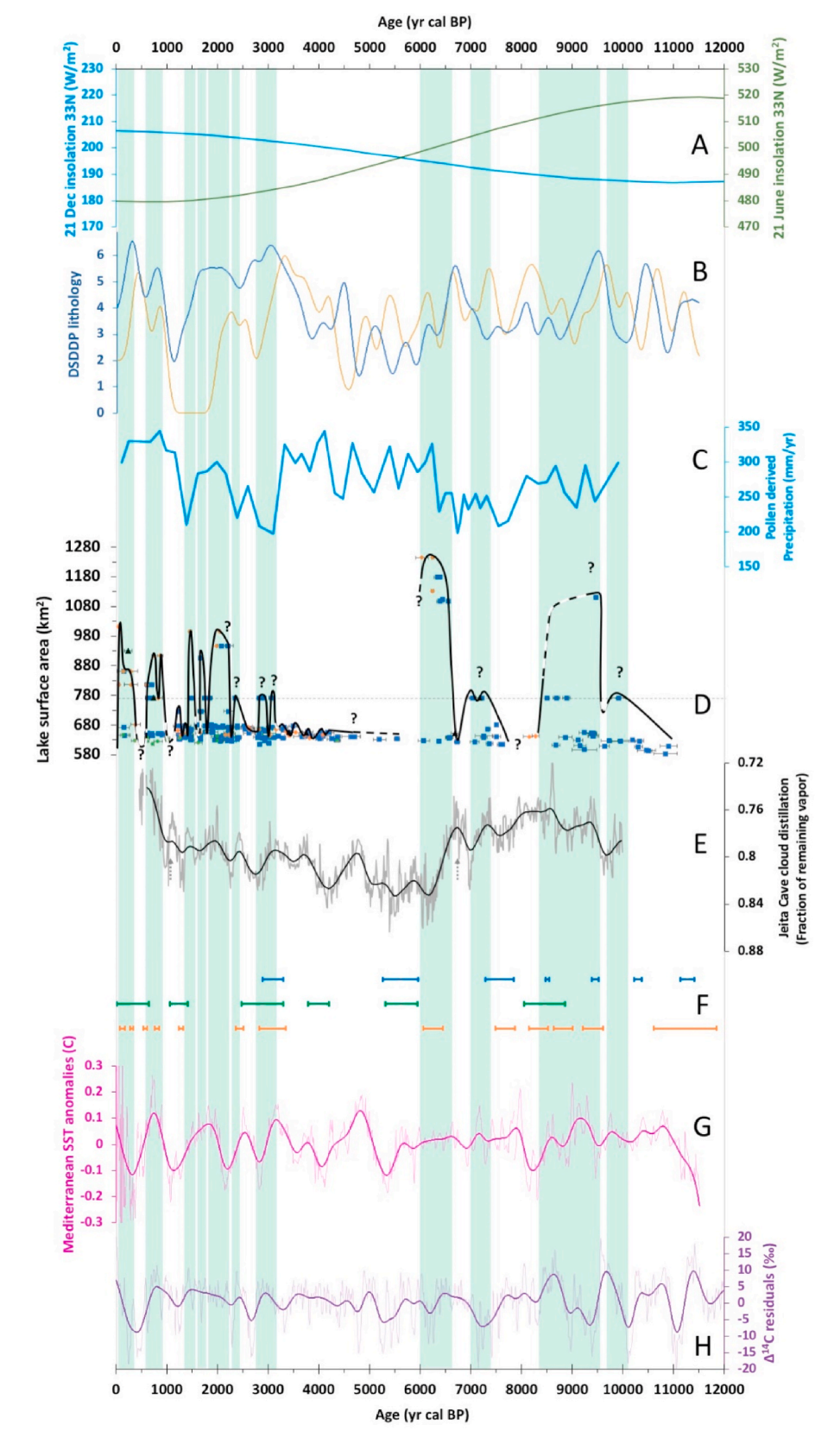


Fig. 5. DS lake-level vs. regional and global records. A) Northern Hemisphere insolation at 33°N during summer (green) and winter (blue)(Paillard et al., 1996). B) lithology of the DSDDP core (0 - air, 1 gravel, 2 - halite, 3 - salty mud, 4 - gypsum, 5 - mud gypsum, 6 - mud, blue line from: Kiro et al., 2016; orange line from: Torfstein et al., 2015). The data was interpolated at 5 year increments and smoothed using a 100 year Gaussian filter. Kiro et al. (2016) created a series of salt sub-categories, for consistency, their lithology was redefined based on the lithological definitions of Torfstein et al. (2015). C) Rainfall reconstruction from DS pollen data (Litt et al., 2012). D) DS lake-surface area history, the data and symbology are the same as in Fig. 4, the lake-area was calculated using the lake hypsometric curve from Fig. 1. E) Jeita Cave cloud distillation (gray line) and 50 year Gaussian smooth (black line) (Gonen and Goldsmith, 2023). Gray arrows indicate times where the Jeita record deviates substantially from the DS lake-level. F) RCC records: Bond cycle (blue lines, times when hematite stained grains from North Atlantic cores were >15%, Bond et al., 2001), periods of high K+ from GISP2 ice core (green lines, Mayewski et al., 2004), advancement of Alps glaciers (orange, times when Alps glaciers were larger than present, (Ivy-Ochs et al., 2009). G) Mediterranean SST residuals, calculated from the Marriner et al. (2022) data by subtracting the raw data from a 400 year Gaussian smooth of the data, and applying a 100 vear Gaussian smooth. H) Intcal20 Δ^{14} C residuals (Reimer et al., 2020) calculated by subtracting the raw data from a 400 year Gaussian smooth of the data (after: Stuiver and Braziunas, 1989) and applying a 100 year Gaussian smooth. Time when the lake was above the sill are marked by green vertical bars.

1 conditions in the Eastern Mediterranean (6.5–5.7 kyr cal BP, De Lange et al., 2008) the decline of the Asian monsoons (5.9 \pm 0.2 kyr cal BP, Goldsmith et al., 2022), and preceded by ~500 years the decline of the African monsoon (5.4 kyr cal BP, Garcin et al., 2017).

From the 6.1-4 kyr cal BP interval there are practically no lake-level indicators from the exposed sediments of the DS. The existing data come from cores along the western margin of the lake recovered from underwater environments (Migowski et al., 2006), and in the later part (since ~4.7 kyr cal BP) also from gypsum deposits in Ein Qedem (Weber et al., 2021), which position the lake-level at around 420 m bsl. In the DSDDP core there are several missing intervals during this time period, which could be related to salt removal during coring, which complicates the ability to assess the lake-status at this time (Fig. 2). In addition, there is a substantial unconformity in Nahal Dagra (Enzel et al., 2000; Kadan, 1997), which current ages constrain between 6 and 2.2 kyr cal BP (Fig. 3). Together, the limited data and unconformity suggest that most probably low lake-levels characterized this time interval. The laminated aragonite layers at 4.6 kyr cal BP in the DSDDP are a possible exception, and likely indicate a somewhat higher lake-level at this time interval. Intriguingly and in contrast to these low levels, the pollen data from the DS shows that the middle Holocene was the wettest of the entire Holocene (Fig. 5)(Litt et al., 2012). This significant discrepancy requires more investigation into effects other than rainfall amount that could be affecting the pollen data.

During the late Holocene, from 4 kyr cal BP onward, the lake-level began rising albeit with fluctuations, and surpassed the sill at $\sim\!3.1$ kyr cal BP (Fig. 4). This lake-level rise and fluctuations were most likely not as large as those documented for the Early Holocene. The DSDDP (Kiro et al., 2020; Neugebauer et al., 2014; Torfstein et al., 2015), the western margin cores (Migowski et al., 2006), and the southern basin cores all contain alternating mud and aragonite layers during the late Holocene; and indicate the reemergence of the wet conditions during this time period. The Medieval Warm Period (1150–750 yr cal BP, Lamb, 1965; Mann et al., 2009), and Little Ice Age (600–250 yr cal BP, Mann et al., 2009) in the DS are characterized by early dry intervals (1200–900 and 600–350 yr cal BP) followed by late wet intervals (900–600 and 350–100 yr cal BP) (Fig. 3). Thus, the timing and hydrological response do not follow the European climate pattern.

The long-term history of the DS shows that the early and late Holocene were predominantly wet albeit punctuated by dry intervals (Fig. 4). The middle Holocene (6.1–3.6 kyr cal BP) was most likely predominantly dry. Overall, wet conditions prevailed in the Levant during both high (early Holocene) and low (late Holocene) north hemisphere summer insolation and it was dry during the transition from maximum to minimum insolation.

4.2. Dead Sea lake-levels vs. regional oxygen isotopic records from speleothems

Oxygen isotopic ($\delta^{18}O_s$) records from Levant speleothems have been interpreted as high-resolution regional hydroclimate records (Bar-Matthews and Ayalon, 2011; Burstyn et al., 2019; Cheng et al., 2015; Keinan et al., 2019). However, a series of Levantine speleothem $\delta^{18} O_{\text{S}}$ records have yielded very different hydroclimate reconstructions from those derived from DS lake-level records (Bar-Matthews et al., 2019; Enzel et al., 2008; Goldsmith et al., 2017b). Recently, Gonen and Goldsmith (2023) proposed a new interpretation of these speleothem records, by considering changes in sea surface temperature, the isotopic composition of the eastern Mediterranean, relative humidity and land temperature and modeled changes in cloud distillation throughout the Holocene (Fig. 5). Cloud distillation (f, percent of remaining vapor in the cloud) represents the integrated magnitude of rainout from the vapor source to the cave, and thus, can be thought of as a measure of integrated rainfall intensity (Goldsmith et al., 2017b). Gonen and Goldsmith (2023) pointed out that the magnitude of distillation from Jeita Cave in Lebanon (Cheng et al., 2015) is very similar to the DS record. Our

updated DS lake-level history presented here, enables an extended view of this potential relation.

It is qualitatively evident that where sufficient DS lake-level data exist, episodes of high lake-levels are also characterized by enhanced distillation (i.e., smaller f, green vertical bars in Fig. 5), and, for the most part, episodes of low lake-levels are characterized by reduced distillation (Fig. 5). This indicates that the Jeita distillation record reconstructs a quite similar hydrological history to that of the DS lake-levels. The Soreq Cave distillation record is highly correlated with the Jeita record ($R^2 = 0.9$, Gonen and Goldsmith, 2023), and thus, these observations hold true also for the Soreq record.

There are a few noticeable exceptions to this observed general relationship between the DS lake-levels and Jeita Cave distillation. A noticeable difference occurs during the early Holocene (10-6 kyr cal BP), where the Jeita record shows a prolonged enhanced distillation interval. During this time interval, the current data shows that the DS lake-level reached its highest stand twice (at 9.5 and 6.5-6 kyr cal BP), and surpassed the sill two additional times (at 9.9 and 7.2 kyr cal BP), unfortunately, the early Holocene record is patchy and is insufficient to assess whether the whole period was wet. There is however, some evidence showing that the lake-level dropped substantially in-between some of the wet phases (at 8.2-8.1 and 6.7 kyr cal BP), also indicated by the salt layers in the DSDDP (Figs. 2 and 5). These drying events (and in particular the 8.2-8.1 kyr cal BPs level drop) are not evident in the Jeita record. The 6.5-6.1 kyr cal BP highstand in the DS is ca. 500 years younger than the potentially corresponding peak in the Jeita record (between 6.9 and 6.5 ky) and might result from a lag time between the rainfall change and the lake drying up. An additional exception are distillation fluctuations between 1400 and 900 years ago, which are not evident in the DS record. More detailed lake-level data from these time intervals are required to further understand these discrepancies.

The Jeita Cave distillation record is a measure of integrated rainfall intensity (Gonen and Goldsmith, 2023), whereas, the lake-level of the DS records a combination of rainfall intensity, rainfall frequency and magnitude of evaporation (e.g., Morin et al., 2019). The overall agreement between the DS lake-level and the Jeita distillation record suggests that throughout much of the Holocene rainfall intensity and total water availability were correlated. As discussed in Gonen and Goldsmith (2023), the Jeita Cave distillation record shows a 10% distillation change throughout the Holocene, whereas the lake-level fluctuations of the DS require a ~50% change in total water availability (Morin et al., 2019). As the Jeita record is a measure of intensity, this would indicate that rainfall intensity is responsible for about 20% of the overall hydrological change and rainfall frequency and evaporation account for the other 80%. Thus, combining results from the DS lake-level with the Jeita Cave distillation reconstruction, provide a quantitative, continuous, high-resolution hydrological reconstruction of the Levant throughout the Holocene. This combined reconstruction allows teasing out and discussing different aspects of rainfall dynamics through time that could not be evaluated otherwise.

4.3. Potential climatic drivers

The DS lake-level and Jeita Cave distillation reconstruction show an intriguing pattern; wet phases in the Levant occurred at times of both high and low summer insolation (early and late Holocene, respectively). This dual wet phase pattern indicates that there were likely two different climatic modes that drove these changes. The existence of a similar dual wet phase pattern during the last interglacial timed similarly (but not identically) in respect to insolation (Goldstein et al., 2020; Kiro et al., 2020; Torfstein et al., 2015) indicates that these two different climatic modes are a typical pattern that characterizes interglacial climates in the Levant. Superimposed on this multi-millennium pattern are large centennial fluctuations that occurred throughout the Holocene. These long- and short-term fluctuations and their potential driving mechanisms are discussed in the next sections.

4.3.1. The Early Holocene

The timing of the high DS levels and enhanced Jeita Cave distillation in the early Holocene (10–6.1 ky) is coeval with high insolation and the Holocene Humid Period (HHP) in tropical regions [e.g., in Africa (Garcin et al., 2017; Shanahan et al., 2015) and East Asia (Goldsmith et al., 2017a)]. The DS lake-level drop at 6.1 kyr cal BP coincides with the termination of sapropel 1 (6.5–5.7 kyr cal BP, De Lange et al., 2008) and the enrichment of Red Sea δ^{18} O (Arz et al., 2003). Empirical evidence suggested that the African monsoon did not propagate all the way into the Levant (Enzel et al., 2015; Palchan and Torfstein, 2019; Quade et al., 2018) and therefore, the moisture was most likely sourced from the Mediterranean (Enzel et al., 2003; Rohling et al., 2015).

The first attempts to explain the wet Early Holocene in the eastern Mediterranean suggested an increase in summer precipitation (Rossignol-Strick, 1987). Since then, the notion of increased summer precipitation during the early Holocene has been challenged on two accounts (Brayshaw et al., 2011; Kutzbach et al., 2014, 2020; Rohling et al., 2015): 1) an increased southeast monsoon in summer during the early Holocene would strengthen the descent of dry air over the eastern Mediterranean and would suppress precipitation to a greater degree than under modern conditions (Brayshaw et al., 2011; Rodwell and Hoskins, 1996; Rohling et al., 2015; Ziv et al., 2004), and 2) model simulations show an increase in winter precipitation and do not show a significant increase in summer precipitation (Brayshaw et al., 2011; Kutzbach et al., 2014, 2020).

The early Holocene winter precipitation increase in the eastern Mediterranean could have been driven by either a dynamic (e.g., shifting of the rain-belts; Enzel et al., 2003) and/or a thermodynamic mechanisms (i.e., lower winter insolation would cause the land to cool more than the ocean and enhance the sea-land temperature gradient during winter). Brayshaw et al. (2011) showed that in time-slice model runs of 8 kyr and 6 kyr, a reduced meridional insolation gradient caused a weakening of the North Atlantic storm-track and a strengthening of the subtropical westerly jet, which caused a southward shift of European rainfall during winter. As a result, precipitation increased in winter over the eastern Mediterranean. This dynamical mechanism of a southward shift of the storm-track is also evident in Kutzbach et al. (2014) model experiment, which examined the precipitation change in the eastern Mediterranean during high and low insolation intervals. Kutzbach et al. (2014) found that a reduced meridional insolation gradient in winter is linked with a southward shift of the westerlies and increased rainfall in the eastern Mediterranean. The Bosmans et al. (2015) model also showed an increase in winter precipitation in the eastern Mediterranean during precession maxima, but they also identified a decrease in the storm-track strength. As a result, they suggest that the increase in precipitation is thermodynamically driven by an enhanced sea-land temperature contrast.

The DS lake-level and Jeita Cave distillation record cannot differentiate between the dynamic and thermodynamic mechanisms. However, the correlation between the two records and the amplification of the DS record in respect to that of the Jeita Cave distillation record, suggests that an increase in rainfall intensity and in rain-storm frequency occurred in tandem. As the model studies presented above did not differentiate between these two aspects of rainfall, it is impossible to evaluate which of the scenarios is more likely. Therefore, we hypothesize that the dynamical mechanism (i.e., a southward shift of the rainbelt) would lead to an increase in the number of rain events and that the thermodynamic mechanism (i.e., increased sea-land contrast) would lead to an increase in rainstorm intensity. The correlation between the two in the proxy records, suggests that both mechanisms potentially operated together to enhance early Holocene precipitation in the eastern Mediterranean.

4.3.2. The Late Holocene

The relatively wet late Holocene (3.6–0 kyr cal BP) in the Levant is intriguing. The modern conditions are a direct continuation of the late

Holocene, and thus, it is reasonable to assume that rainfall throughout the late Holocene occurred during winter. The conditions prior to the industrial revolution saw a cooling ocean and increased winter insolation, which would decrease the sea-land temperature contrast and reduce precipitation. Thus, a simple thermodynamic mechanism is not viable to explain the rise of the DS lake-level, and some flavor of a dynamic mechanism is most likely responsible for this wetting trend. The question of what drives modern rainfall variability in the Levant is currently being debated (e.g., Garfinkel et al., 2020; Hochman et al., 2018; Seager et al., 2014; Tuel and Eltahir, 2020), making the interpretation of past changes a challenge. Kushnir and Stein (2010) suggested that cold north Atlantic SSTs cause a large positive sea level pressure anomaly over the midlatitude North Atlantic, raising the likelihood of cold air outbreaks and cyclogenesis in the eastern Mediterranean and therefore the occurrence of more rainfall in the Levant. The progressive cooling of the tropical North Atlantic throughout the late Holocene (Marcott et al., 2013) along with the rise in DS lake-levels is consistent with this mechanism. Interestingly, Brayshaw et al. (2011) time slice model of the Holocene showed a rainfall increase in the eastern Mediterranean between 3 and 1 ky to levels similar to that of the early Holocene, in line with DS lake-levels, however, a mechanism was not presented in their paper.

4.3.3. Centennial-millennial scale events

The Holocene DS record can be viewed in two ways. The first, presented above, is that of a record that exhibits a multi-millennia scale periodicity, where the early (10–6 kyr cal BP) and late Holocene (3.6–0 kyr cal BP) were wet and the middle Holocene (6–3.6 kyr cal BP) was dry. This type of variability indicates that the long-term paleohydrology is governed by radiative forcings (e.g. insolation, greenhouse gases, etc.) as suggested for the monsoonal regions (e.g. Garcin et al., 2017; Goldsmith et al., 2017a; Haug et al., 2001). The second way to view the DS record is that of a series of rapid climate changes (RCC's) at a decadal to centennial scale that entail substantial hydrological changes (~50% in mean annual rainfall). In previous paragraphs we explored the former option, in the paragraph below, we explore the latter.

We plotted some of the canonical RCC records (e.g., Bond et al., 1997; Mayewski et al., 2004; Solomina et al., 2015) and compared them with the DS lake-level fluctuations (Fig. 5). It is hard to recognize a systematic relationship between the DS lake-levels and these RCCs. The centennial to millennial fluctuations in the DS lake-level seem to correspond, at least for the most part, with 1) the Δ^{14} C residuals [calculated as the residuals of a 400 year Gaussian smoothed of Incal20 (Reimer et al. (2020) following the method of: Stuiver and Braziunas (1989)], which have been interpreted as a proxy for solar oscillations (Stuiver and Braziunas, 1989), and 2) Mediterranean SST anomalies [calculated as the residuals of a 400 year Gaussian smoothed average of the Mediterranean SST from Marriner et al. (2022), Fig. 5]. Kushnir and Stein (2019) identified the temporal association between the DS lake-levels and proxies of solar irradiance oscillations (associated with changes in solar magnetic activity) over the past 1500 years. Our new and extended DS record confirms that this linkage of low (high) solar irradiance and cold (warm) Mediterranean SST anomalies with low (high) DS lake-levels, may hold for the whole Holocene, with a potential discrepancy of the 6.5 kyr cal BP highstand (Fig. 5). The Jeita distillation record also shows a remarkable resemblance with the Δ^{14} C residuals and SST anomaly, with notable exceptions at 8.1 and 6.5 kyr cal BP (Fig. 5). Kushnir and Stein (2019) proposed a mechanism that links Δ^{14} C residuals, Mediterranean SST anomalies and the DS lake-level, where reduced solar irradiance causes colder winters (colder SSTs) and a western expansion of the Siberian High, which prevents Atlantic Ocean moisture from entering the Levant and causes dry conditions. The similarity between the Δ^{14} C residuals, SST anomalies and the DS lake-level is most evident for the late Holocene (<3.6 kyr cal BP), and is less pronounced during the early and middle Holocene. This might suggest that during the early and late Holocene the DS lake-levels responded

differently to changes in solar insolation and Mediterranean SST.

4.4. Proposing archaeological implications

The Levant, a locus of some of the most dramatic cultural changes in human history (e.g. the onset of sedentism, agriculture and urbanization, Bar-Yosef and Belfer-Cohen, 1989; Greenberg, 2019), is located at the northern boundary of the global desert belt, and is characterized by high spatial variability of storms and annual rainfall totals (e.g., Enzel et al., 2008) making it a climatically fragile region (Ellenblum, personal communication). In such a region, small changes in water availability could incur substantial ecological and agricultural changes across the landscape and in turn, cultural responses (Peleg et al., 2012). The DS provides a quantitative hydroclimate record of the Levant and thus can be used to assess the potential role of climate in the region's cultural evolution. As we are not archaeologists, we will not try to interpret the material culture in light of the hydroclimate reconstruction; however, we would like to evaluate whether there are possible relations between regional water availability and population dynamics.

To assess the history of cultural change in the Levant, we use the results of the archaeological site number database (Palmisano et al., 2019), which contains 20,688 sites of the different cultural entities throughout the Holocene (12-0.5 kyr cal BP)(Fig. 6). We acknowledge that the number of sites is probably not the best metric for evaluating population size because (Drennan et al., 2015): 1) it does not account for the size of the sites, 2) it might be biased towards time intervals that are more highly studied (e.g., the "Biblical Period" of the Iron Age), 3) it does not consider the potential destruction of sites through time (i.e., the older the site, the higher the chances it will be destroyed), and 4) the site number data compiled is based on many surveys that did not use a standardized definition of a "site" (e.g., is a site defined as a scatter of pottery or as a city?), and therefore, the self-consistency is unclear. Therefore, once a more detailed database of site size and results of systematic surveys is constructed, the relations presented below should be reevaluated. In addition, the raw data are not available in the Palmisano et al. (2019) paper. In light of these issues, we present a simplistic view of population dynamics, using the summary plot of Palmisano et al. (2019). For each cultural entity, we evaluate whether population increased or decreased, in respect to the previous entity. As the Palmisano et al. (2019) database does not contain information

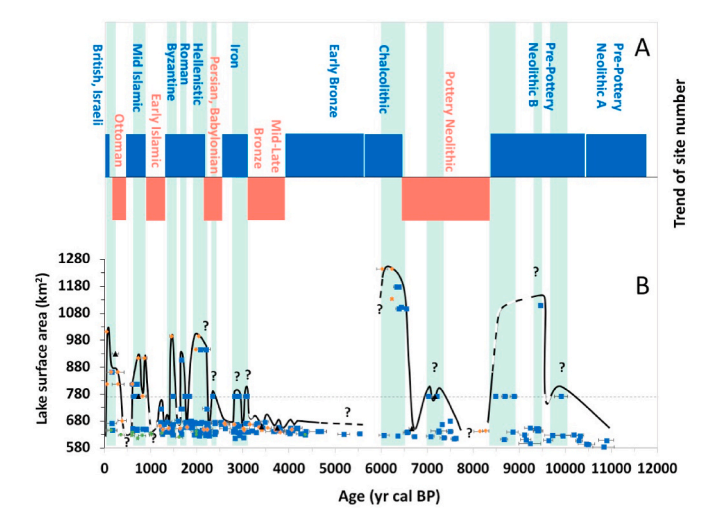


Fig. 6. DS lake-level data vs. trend of archaeological site number in the Levant. A) The trend of archaeological site number in the Levant (after: Palmisano et al., 2019). For each cultural entity, we evaluate whether the number of sites increased (blue) or decreased (red), in respect to the previous entity. B) Dead Sea lake-level, see Fig. 4 for details. Time when the lake was above the sill are marked by green vertical bars.

regarding the past 500 years, we use the description from Lewis (1954) of a population increase from the Middle Islamic period to the Ottoman Period. The chronology and duration of each entity is based on Palmisano et al. (2019).

The site number trend, qualitatively compared with the DS lake-area (Fig. 6), shows an overall relation. During intervals when the lake is large there is a site increase (during the Pre-pottery Neolithic B, Chalcolithic, Iron, Hellenistic - Roman – Byzantine, Middle Islamic, and British – Israeli) and during intervals when the lake is low there is a site decrease (during the Pottery Neolithic, Persian – Babylonian, Early Islamic and Ottoman). There are also exceptions that do not fit this relation (the Pre-Pottery Neolithic A and the Early Bronze Age). The relation presented, though crude, does suggest potential linkages between population dynamics and hydroclimate variability. More detailed and nuanced information pertaining to temporal leads or lags between the two datasets and a better quantification of both datasets is required to better understand this relation through time.

An additional important observation that is evident from this comparison, regards the collapse of the Late Bronze Age at 3200 years BP, which has been suggested to have been driven by a climatic shift (e.g., Langgut et al., 2014). This suggestion was supported by the DS lake-level record, and in particular the earlier interpretation and dating (of \sim 3.6 kyr cal BP) of the Ein Gedi high-stand sequence (Bartov, 2004; Langgut et al., 2014; Migowski et al., 2006). Our reevaluation of the ages from the Ein Gedi sequence questions the 3.6 kyr cal BP age (Bartov, 2004), and thus, we did not use this data point. Without this single point, it can be concluded that the lake-level begun rising at 4 kyr cal BP and overtopped the sill at 3.1 kyr cal BP. A similar pattern is identified in the Jeita Cave record, where lower distillation characterized the first half of the Late Bronze Age, and a gradual distillation increase occurred throughout the Late Bronze Age and into Iron Age I. Thus, the transition from the Late Bronze Age into Iron Age I in the Levant was characterized by a wetting trend, and not drying.

4.5. Implications for Levant climate under global warming

The combined records from the DS and Jeita Cave provide a more complete account of the natural hydroclimate variability in the Levant, and thus provide additional means for evaluating the significance of predicted future hydroclimate changes in respect to the background natural variability. Global circulation models (GCM) predict a 40% rainfall decline (a decline of ca. ${\sim}200~\text{mm/yr})$ under the RCP4.5 scenario by the end of the century due to global warming, which results in a drying rate of \sim 2 mm/yr over the next century (Hochman et al., 2018). The Jeita Cave record points to a secular rainfall increase throughout the past 3 kyr cal BP and the DS shows wetter conditions than the middle Holocene. To evaluate the significance of natural variability in respect to predicted anthropogenic changes, we used the sensitivity of DS lake-level to rainfall changes from Morin et al. (2019). This 30 m lake-level rise (from 420 to 390 m bsl between 3 ky to present) requires a rainfall increase of ~500 mm/yr, which took ~3 kyr, i.e. an average rainfall increase of ~ 0.2 mm/year. Thus, the predicted hydroclimate change due to anthropogenic global warming is an order of magnitude larger than the natural hydroclimate trend, indicating that the natural rainfall increase will be overwhelmed by the global-warming induced drying.

The largest sub-millennial fluctuations of the lake (e.g., at 500 years BP), which are reflected by rising and falling lake-levels, require rainfall fluctuation rates of 2-3 mm/yr (~ 500 mm/yr change that occurred over a period of ~ 200 years), which are similar to the rate predicted for future drying. As the drivers and frequency of the sub-millennial scale lake-level fluctuations are not well understood, it is unclear where current rainfall is placed in these wetting and drying cycles, and thus, whether natural variability is working to amplify the global warming drying or to attenuate it. Higher resolution transient models are required to potentially tackle the frequency and phasing of these potential sub-

millennial scale fluctuations and attempt to resolve these issues.

5. Conclusions

We reconstructed the DS lake-level changes throughout the Holocene using: 1) new data regarding the high-stands of the lake derived from three cores collected in the DS southern basin, 2) a re-evaluation and dating of the two major Holocene high-stand exposures, and 3) a compilation of all previously dated (n=296 radiocarbon ages) Holocene DS lake status records. Using these data, we draw the following conclusions:

- 1) The early (10–6.1 kyr cal BP) and late Holocene (3.6–0 kyr cal BP) in the DS were predominantly wet and were also characterized by relatively large lake-level fluctuations, whereas the middle Holocene (6.1–3.6 kyr cal BP) was most likely dry.
- 2) The pattern of dual humid periods in the Holocene is also evident in the Jeita Case distillation record from Lebanon (which represents the integrated magnitude of rainout from the vapor source to the cave). In tandem, these two records provide a quantitative, continuous high-resolution hydrological reconstruction of the Levant throughout the Holocene and indicate that rainfall intensity and total water availability were correlated throughout the Holocene.
- 3) Wet phases in the Levant occurred at times of both high and low summer insolation (early and late Holocene, respectively). This dual humid pattern suggests that there are most likely two different climatic modes that drove these changes. Both dynamic (e.g., shifting of the rain-belts) and/or a thermodynamic (i.e., increased land-sea temperature gradient) mechanisms could have driven these changes. High-resolution transient models are required to tease out these two possible mechanisms.
- 4) There are associations that can be drawn between the DS lake-level fluctuations and cultural transitions in the Levant. These provide a basis for investigating cultural responses to different background climatic conditions.
- 5) The DS lake-level record shows that the natural variability of water availability in the Levant is large, and therefore, this region is highly sensitive to global climatic changes. The predicted future change is of similar magnitude to the natural climate variability and thus, it is crucial to assess whether the anthropogenic drying conditions are inor out-of phase with the natural climate variability in this region.

Funding

This research was funded by: an Israel Science Foundation grant no. 2229/2, a Hebrew University Center for Sustainability Grant, a US-Israel Binational Science Foundation grant no. USIBSF 2020364 and a US National Science foundation grant no. AGS 21-27684.

Author contribution

Yonaton Goldsmith: Conceptualization, Methodology, Formal analysis, Investigation, Resources, Data Curation, Writing - Original Draft, Writing - Review & Editing, Visualization, Funding acquisition. Ofer Cohen: Formal analysis, Software, Visualization. Mordechai Stein: Validation, Methodology, Investigation, Writing - Review & Editing. Adi Torfstein: Formal analysis, Methodology, Investigation, Writing - Review & Editing, Funding acquisition. Yael Kiro: Methodology, Investigation, Writing - Review & Editing. Yochanan Kushnir: Investigation, Writing - Review & Editing. Yuval Bartov: Formal analysis, Investigation, Writing - Review & Editing. Liran Ben-Moshe: Formal analysis. Amos Frumkin: Formal analysis, Investigation, Validation. Nadav Lensky: Investigation, Validation. Jonathan Keinan: Formal analysis, Investigation. Lilach Gonen: Formal analysis, Investigation. Yehouda Enzel: Conceptualization, Methodology, Formal analysis, Investigation, Resources, Writing - Review & Editing, Funding acquisition.

Declaration of competing interest

The authors declare that they have no known competing financial interests or personal relationships that could have appeared to influence the work reported in this paper.

Data availability

All data in this article is presented in the supplementary material.

Acknowledgements

We would like to thank: Efrat Morin, John Southon, Yitzchak Jaffe, Uri Davidovich, Ido Wachtel, Oren Kolodny, Uri Ryb, Revital Ken-Tor Bookman, Elisa Kagan and Joseph Charrach for fruitful discussions regarding different aspects of this research and Nathan Sheffer, Amit Kas and Ofir Bacar from the DSW for their help with acquiring the southern basin cores. We thank QSR handling Editor Prof. Patrick Rioual and the two anonymous reviewers for their insightful comments that helped improve the manuscript.

Appendix A. Supplementary data

Supplementary data to this article can be found online at https://doi.org/10.1016/j.quascirev.2023.108312.

References

- Al-Zoubi, A., ten Brink, U.S., 2001. Salt diapirs in the Dead Sea basin and their relationship to Quaternary extensional tectonics. Mar. Petrol. Geol. 18, 779–797. https://doi.org/10.1016/S0264-8172(01)00031-9.
- Arz, H.W., Lamy, F., P\u00e4ztzold, J., M\u00fciller, P.J., Prins, M., 2003. Mediterranean moisture source for an early-holocene Humid Period in the northern Red Sea. Science (80-300, 118-121. https://doi.org/10.1126/science.1080325.
- Bar-Matthews, M., Ayalon, A., 2011. Mid-holocene climate variations revealed by high-resolution speleothem records from Soreq cave, Israel and their torrelation with cultural changes. Holocene 21, 163–171. https://doi.org/10.1177/0959683610384165.
- Bar-Matthews, M., Keinan, J., Ayalon, A., 2019. Hydro-climate research of the late quaternary of the Eastern Mediterranean-Levant region based on speleothems research – a review. Quat. Sci. Rev. 221, 105872 https://doi.org/10.1016/j. quascirev.2019.105872.
- Bar-Yosef, O., Belfer-Cohen, A., 1989. The origins of sedentism and farming communities in the Levant. J. World PreHistory 3, 447–498. https://doi.org/10.1007/ BF00975111.
- Bartov, Y., 2004. Unpubl. PhD. Thesis. In: Sedimentary Fill Analysis of a Continental Basin—The Late Pleistocene Dead Sea. The Hebrew University of Jerusalem.
- Bartov, Y., Agnon, A., Enzel, Y., Stein, M., 2006. Late Quaternary faulting and subsidence in the central Dead Sea basin. Isr. J. Earth Sci. 55, 18–31. https://doi.org/10.1560/ K74U-0772-1642-6282.
- Bartov, Y., Goldstein, S.L., Stein, M., Enzel, Y., 2003. Catastrophic arid episodes in the eastern mediterranean linked with the North Atlantic heinrich events. Geology 31, 439. https://doi.org/10.1130/0091-7613(2003)031<0439:CAEITE>2.0.CO:2.
- Bartov, Y., Stein, M., Enzel, Y., Agnon, A., Reches, Z., 2002. Lake levels and sequence stratigraphy of Lake lisan, the late Pleistocene precursor of the Dead Sea. Quat. Int. 57, 9–21. https://doi.org/10.1006/gres.2001.2284.
- Ben Dor, Y., Neugebauer, I., Enzel, Y., Schwab, M.J., Tjallingii, R., Erel, Y., Brauer, A., 2019. Varves of the Dead Sea sedimentary record. Quat. Sci. Rev. 215, 173–184. https://doi.org/10.1016/j.quascirev.2019.04.011.
- Benson, L., Paillet, F.L., 1989. The use of total lake-surface area as an indicator of climatic change; examples from the lahontan basin. Ouat. Res. 32, 262–275.
- Bond, G., Kromer, B., Beer, J., Muscheler, R., Evans, M.N., Showers, W., Hoffmann, S., Lotti-Bond, R., Hajdas, I., Bonani, G., 2001. Persistent solar influence on North Atlantic climate during the Holocene. Science 294, 2130–2136. https://doi.org/ 10.1126/science.1065680.
- Bond, G., Showers, W., Cheseby, M., Lotti, R., Almasi, P., DeMenocal, P., Priore, P., Cullen, H., Hajdas, I., Bonani, G., 1997. A pervasive millennial-scale cycle in North Atlantic Holocene and glacial climates. Science 278, 1257–1266. https://doi.org/10.1126/science.278.5341.1257.
- Bookman, R., Enzel, Y., Agnon, A., Stein, M., 2004. Late Holocene lake levels of the Dead Sea. Geol. Soc. Am. Bull. 116, 555–571. https://doi.org/10.1130/B25286.1.
- Bosmans, J.H.C., Drijfhout, S.S., Tuenter, E., Hilgen, F.J., Lourens, L.J., Rohling, E.J., 2015. Precession and obliquity forcing of the freshwater budget over the Mediterranean. Quat. Sci. Rev. 123, 16–30. https://doi.org/10.1016/j. quascirev.2015.06.008.

- Brayshaw, D.J., Rambeau, C.M.C., Smith, S.J., 2011. Changes in Mediterranean climate during the Holocene: insights from global and regional climate modelling. Holocene 21, 15–31. https://doi.org/10.1177/0959683610377528.
- Broecker, W.S., 2010. Long-term water prospects in the western United States. J. Clim. 23, 6669–6683. https://doi.org/10.1175/2010JCLI3780.1.
- Broecker, W.S., Orr, P.C., 1958. Radiocarbon chronology of lake lahontan and lake bonneville. Bull. Geol. Soc. Am. 69, 1009–1032. https://doi.org/10.1130/0016-7606(1958)69[1009:RCOLLA]2.0.CO;2.
- Burstyn, Martrat, Lopez, Iriarte, Jacobson, Lone, Deininger, 2019. Speleothems from the Middle East: an example of water limited environments in the SISAL database. Quaternary 2, 16. https://doi.org/10.3390/quat2020016.
- Charrach, J., 2019. Investigations into the Holocene geology of the Dead Sea basin.

 Carbonates Evaporites 34, 1415–1442. https://doi.org/10.1007/s13146-018-0454-
- Cheng, H., Sinha, A., Verheyden, S., Nader, F.H., Li, X.L., Zhang, P.Z., Yin, J.J., Yi, L., Peng, Y.B., Rao, Z.G., Ning, Y.F., Edwards, R.L., 2015. The climate variability in northern Levant over the past 20,000 years. Geophys. Res. Lett. 42, 8641–8650. https://doi.org/10.1002/2015GL065397.
- De Lange, G.J., Thomson, J., Reitz, A., Slomp, C.P., Speranza Principato, M., Erba, E., Corselli, C., 2008. Synchronous basin-wide formation and redox-controlled preservation of a Mediterranean sapropel. Nat. Geosci. 1, 606–610. https://doi.org/10.1038/ngeo283.
- Drennan, R.D., Peterson, C.E., Berrey, C.A., 2015. Regional Settlement Demography in Archaeology. ISD, Bristol, CT (USA).
- Ebert, Y., Shaar, R., Stein, M., 2021. Decadal geomagnetic secular variations from greigite bearing Dead Sea sediments. Geochem., Geophys. Geosyst. 22, 1–15. https://doi.org/10.1029/2021GC009665.
- Enzel, Y., 1992. Flood frequency of the Mojave River and the formation of late Holocene playa lakes. Holocene 2, 11–18.
- Enzel, Y., Amit, R., Dayan, U., Crouvi, O., Kahana, R., Ziv, B., Sharon, D., 2008. The climatic and physiographic controls of the eastern Mediterranean over the late Pleistocene climates in the southern Levant and its neighboring deserts. Global Planet. Change 60, 165–192. https://doi.org/10.1016/j.gloplacha.2007.02.003.
- Enzel, Y., Bookman, R., Sharon, D., Gvirtzman, H., Dayan, U., Ziv, B., Stein, M., 2003. Late Holocene climates of the Near East deduced from Dead Sea level variations and modern regional winter rainfall. Quat. Res. 60, 263–273. https://doi.org/10.1016/j.vgres.2003.07.011.
- Enzel, Y., Kadan, G., Eyal, Y., 2000. Holocene earthquakes inferred from a fan-delta sequence in the Dead Sea graben. Quat. Res. 53, 34–48. https://doi.org/10.1006/ gres.1999.2096.
- Enzel, Y., Kushnir, Y., Quade, J., 2015. The middle Holocene climatic records from Arabia: reassessing lacustrine environments, shift of ITCZ in Arabian Sea, and impacts of the southwest Indian and African monsoons. Global Planet. Change 129, 69–91. https://doi.org/10.1016/j.gloplacha.2015.03.004.
- Enzel, Y., Mushkin, A., Groisman, M., Calvo, R., Eyal, H., Lensky, N., 2022. The modern wave-induced coastal staircase morphology along the western shores of the Dead Sea. Geomorphology 408, 108237. https://doi.org/10.1016/j. geomorph.2022.108237.
- Frumkin, A., Kadan, G., Enzel, Y., Eyal, Y., 2001. Radiocarbon chronology of the Holocene Dead Sea: attempting a regional correlation. Radiocarbon 43, 1179–1189. https://doi.org/10.1017/S0033822200038479.
- Garcin, Y., Schildgen, T.F., Torres Acosta, V., Melnick, D., Guillemoteau, J., Willenbring, J., Strecker, M.R., 2017. Short-lived increase in erosion during the african Humid Period: evidence from the northern Kenya rift. Earth Planet Sci. Lett. 459, 58–69. https://doi.org/10.1016/j.epsl.2016.11.017.
- Garfinkel, C.I., Adam, O., Morin, E., Enzel, Y., Elbaum, E., Bartov, M., Rostkier-Edelstein, D., Dayan, U., 2020. The role of zonally averaged climate change in contributing to intermodel spread in CMIP5 predicted local precipitation changes. J. Clim. 33, 1141–1154. https://doi.org/10.1175/JCLI-D-19-0232.1.
- Goldsmith, Y., Broecker, W.S., Xu, H., Polissar, P.J., DeMenocal, P.B., Porat, N., Lan, J., Cheng, P., Zhou, W., An, Z., 2017a. Northward extent of East Asian monsoon covaries with intensity on orbital and millennial timescales. Proc. Natl. Acad. Sci. 114, 1817–1821. https://doi.org/10.1073/pnas.1616708114.
- Goldsmith, Y., Polissar, P.J., Ayalon, A., Bar-Matthews, M., DeMenocal, P.B., Broecker, W.S., 2017b. The modern and Last Glacial Maximum hydrological cycles of the Eastern Mediterranean and the Levant from a water isotope perspective. Earth Planet Sci. Lett. 457, 302–312. https://doi.org/10.1016/j.epsl.2016.10.017.
- Goldsmith, Y., Xu, H., Torfstein, A., Lan, J., Song, Y., Zhang, J., Zhou, K., Cheng, J., Enzel, Y., 2022. Abrupt contraction of the indo-east asian monsoons ended the Holocene Humid Period. Geophys. Res. Lett. 49, 1–10. https://doi.org/10.1029/ 2022GL100137.
- Goldstein, S.L., Kiro, Y., Torfstein, A., Kitagawa, H., Tierney, J., Stein, M., 2020. Revised chronology of the ICDP Dead Sea deep drill core relates drier- wetter-drier climate cycles to insolation over the past 220 kyr. Quat. Sci. Rev. 244, 106460 https://doi. org/10.1016/j.quascirev.2020.106460.
- Gonen, L., Goldsmith, Y., 2023. Middle Eastern cloud distillation throughout the Holocene - quantified using oxygen isotopes from speleothems and deep-sea cores. Quat. Sci. Rev. 307, 108053 https://doi.org/10.1016/j.quascirev.2023.108053.
- Greenberg, R., 2019. The Archaeology of the Bronze Age Levant. Cambridge University Press. https://doi.org/10.1017/9781316275993.
- Haase-Schramm, A., Goldstein, S.L., Stein, M., 2004. U-Th dating of Lake Lisan (late Pleistocene dead sea) aragonite and implications for glacial east Mediterranean climate change. Geochim. Cosmochim. Acta 68, 985–1005. https://doi.org/ 10.1016/j.gca.2003.07.016.

- Haliva-Cohen, A., Stein, M., Goldstein, S.L., Sandler, A., Starinsky, A., 2012. Sources and transport routes of fine detritus material to the Late Quaternary Dead Sea basin. Quat. Sci. Rev. 50, 55–70. https://doi.org/10.1016/j.quascirev.2012.06.014.
- Haug, G.H., Hughen, K.A., Sigman, D.M., Peterson, L.C., Röhl, U., 2001. Southward migration of the intertropical convergence zone through the Holocene. Science (80-293, 1304–1308. https://doi.org/10.1126/science.1059725.
- Hirschfeld, Y., 2006. The archaeology of the Dead Sea valley in the late hellenistic and early roman periods. Spec. Pap. Geol. Soc. Am. 401, 215–229. https://doi.org/ 10.1130/2006.2401(14.
- Hochman, A., Mercogliano, P., Alpert, P., Saaroni, H., Bucchignani, E., 2018. High-resolution projection of climate change and extremity over Israel using COSMO-CLM. Int. J. Climatol. 38, 5095–5106. https://doi.org/10.1002/joc.5714.
- Ivy-Ochs, S., Kerschner, H., Maisch, M., Christl, M., Kubik, P.W., Schlüchter, C., 2009. Latest Pleistocene and Holocene glacier variations in the European Alps. Quat. Sci. Rev. 28, 2137–2149. https://doi.org/10.1016/j.quascirev.2009.03.009.
- Kadan, G., 1997. The Holocene Fan-Delta of Nahal Darga, Israel. Unpubl. M.Sc. Thesis. In: Evidence for Dead Sea Lake-Level Fluctuations and Recent Tectonism from. Ben-Gurion University of the Negev, Beer-Sheva.
- Kagan, E., Stein, M., Agnon, A., Neumann, F., 2011. Intrabasin paleoearthquake and quiescence correlation of the late Holocene Dead Sea. J. Geophys. Res. Solid Earth 116, 1–27. https://doi.org/10.1029/2010JB007452.
- Kagan, E.J., Langgut, D., Boaretto, E., Herald Neumann, F., Stein, M., 2015. Dead Sea levels during the Bronze and Iron ages. Radiocarbon 57, 237–252. https://doi.org/ 10.2458/azu rc.57.18560.
- Keinan, J., Bar-Matthews, M., Ayalon, A., Zilberman, T., Agnon, A., Frumkin, A., 2019. Paleoclimatology of the levant from zalmon cave speleothems, the northern Jordan valley, Israel. Quat. Sci. Rev. 220, 142–153. https://doi.org/10.1016/j. quascirev.2019.07.018.
- Kiro, Y., Goldstein, S.L., Kushnir, Y., Olson, J.M., Bolge, L., Lazar, B., Stein, M., 2020. Droughts, flooding events, and shifts in water sources and seasonality characterize last interglacial Levant climate. Quat. Sci. Rev. 248, 106546 https://doi.org/ 10.1016/j.quascirev.2020.106546.
- Kiro, Y., Goldstein, S.L., Lazar, B., Stein, M., 2016. Environmental implications of salt facies in the Dead Sea. Geol. Soc. Am. Bull. 128, 824–841. https://doi.org/10.1130/ B31357 1
- Kitagawa, H., Stein, M., Goldstein, S.L., Nakamura, T., Lazar, B., 2017. Radiocarbon chronology of the DSDDP core at the deepest floor of the Dead Sea. Radiocarbon 59, 383–394. https://doi.org/10.1017/RDC.2016.120.
- Klein, C., Flohn, H., 1987. Contributions to the knowledge of the fluctuations of the Dead Sea level. Theor. Appl. Climatol. 38, 151–156. https://doi.org/10.1007/
- Kushnir, Y., Stein, M., 2019. Medieval climate in the eastern mediterranean: instability and evidence of solar forcing. Atmosphere 10, 29. https://doi.org/10.3390/ atmos10010029
- Kushnir, Y., Stein, M., 2010. North Atlantic influence on 19th–20th century rainfall in the Dead Sea watershed, teleconnections with the Sahel, and implication for Holocene climate fluctuations. Quat. Sci. Rev. 29, 3843–3860. https://doi.org/ 10.1016/j.quascirev.2010.09.004.
- Kutzbach, J.E., Chen, G., Cheng, H., Edwards, R.L., Liu, Z., 2014. Potential role of winter rainfall in explaining increased moisture in the Mediterranean and Middle East during periods of maximum orbitally-forced insolation seasonality. Clim. Dynam. 42, 1079–1095. https://doi.org/10.1007/s00382-013-1692-1.
- Kutzbach, J.E., Guan, J., He, F., Cohen, A.S., Orland, I.J., Chen, G., 2020. African climate response to orbital and glacial forcing in 140,000-y simulation with implications for early modern human environments. Proc. Natl. Acad. Sci. 117, 2255–2264. https:// doi.org/10.1073/pnas.1917673117.
- Lamb, H.H., 1965. The early medieval warm epoch and its sequel. Palaeogeogr. Palaeoclimatol. Palaeoecol. 1, 13–37. https://doi.org/10.1016/0031-0182(65) 90004-0.
- Langgut, D., Neumann, F.H., Stein, M., Wagner, A., Kagan, E.J., Boaretto, E., Finkelstein, I., 2014. Dead Sea pollen record and history of human activity in the judean highlands (Israel) from the intermediate Bronze into the Iron ages (~2500-500 BCE). Palynology 38, 280–302. https://doi.org/10.1080/ 01916122 2014 906001
- Lewis, B., 1954. Studies in the ottoman archives—I. Bull. Sch. Orient. African Stud. 16, 469–501. https://doi.org/10.1017/S0041977X00086808.
- Litt, T., Ohlwein, C., Neumann, F.H., Hense, A., Stein, M., 2012. Holocene climate variability in the Levant from the Dead Sea pollen record. Quat. Sci. Rev. 49, 95–105. https://doi.org/10.1016/j.quascirev.2012.06.012.
- Liu, T., Broecker, W.S., Stein, M., 2013. Rock varnish evidence for a Younger Dryas wet period in the Dead Sea basin. Geophys. Res. Lett. 40, 2229–2235. https://doi.org/ 10.1002/grl.50492.
- Ludwig, K.R., 2003. Mathematical-statistical treatment of data and errors for 230 Th/U geochronology. In: Uranium-Series Geochemistry. De Gruyter, pp. 631–656. https://doi.org/10.1515/9781501509308-021.
- Mann, M.E., Zhang, Z., Rutherford, S., Bradley, R.S., Hughes, M.K., Shindell, D., Ammann, C., Faluvegi, G., Ni, F., 2009. Global signatures and dynamical origins of the little ice age and medieval climate anomaly. Science 326, 1256–1260. https:// doi.org/10.1126/science.1177303.
- Marcott, S.a., Shakun, J.D., Clark, P.U., Mix, A.C., 2013. A reconstruction of regional and global temperature for the past 11,300 years. Science 339, 1198–1201. https://doi. org/10.1126/science.1228026.
- Marriner, N., Kaniewski, D., Pourkerman, M., Devillers, B., 2022. Anthropocene tipping point reverses long-term Holocene cooling of the Mediterranean Sea: a meta-analysis of the basin's Sea Surface Temperature records. Earth Sci. Rev. 227, 103986 https:// doi.org/10.1016/j.earscirev.2022.103986.

- Mayewski, P. a, Rohling, E.E., Curt Stager, J., Karlén, W., Maasch, K.A., Meeker, L.D., Meyerson, E.A., Gasse, F., van Kreveld, S., Holmgren, K., Lee-Thorp, J., Rosqvist, G., Rack, F., Staubwasser, M., Schneider, R.R., Steig, E.J., 2004. Holocene climate variability. Quat. Res. 62, 243–255. https://doi.org/10.1016/j.yqres.2004.07.001.
- McGee, D., Moreno-Chamarro, E., Marshall, J., Galbraith, E.D., 2018. Western U.S. lake expansions during Heinrich stadials linked to Pacific Hadley circulation. Sci. Adv. 4, 1–11. https://doi.org/10.1126/sciadv.aav0118.
- Migowski, C., Stein, M., Prasad, S., Negendank, J.F.W., Agnon, A., 2006. Holocene climate variability and cultural evolution in the Near East from the Dead Sea sedimentary record. Quat. Res. 66, 421–431. https://doi.org/10.1016/j. yqres.2006.06.010.
- Morin, E., Ryb, T., Gavrieli, I., Enzel, Y., 2019. Mean, variance, and trends of Levant precipitation over the past 4500 years from reconstructed Dead Sea levels and stochastic modeling. Quat. Res. 91, 751–767. https://doi.org/10.1017/qua.2018.98.
- Neev, D., Emery, K.O., 1967. The Dead Sea: Depositional Processes and Environments of Evaporites. Israel Geological Survey, Jerusalem.
- Neugebauer, I., Brauer, A., Schwab, M.J., Waldmann, N.D., Enzel, Y., Kitagawa, H., Torfstein, A., Frank, U., Dulski, P., Agnon, A., Ariztegui, D., Ben-Avraham, Z., Goldstein, S.L., Stein, M., 2014. Lithology of the long sediment record recovered by the ICDP Dead Sea Deep drilling Project (DSDDP). Quat. Sci. Rev. 102, 149–165. https://doi.org/10.1016/j.quascirev.2014.08.013.
- Neumann, F.H., Kagan, E.J., Schwab, M.J., Stein, M., 2007. Palynology, sedimentology and palaeoecology of the late Holocene Dead Sea. Quat. Sci. Rev. 26, 1476–1498. https://doi.org/10.1016/j.quascirev.2007.03.004.
- Paillard, D., Labeyrie, L., Yiou, P., 1996. Macintosh Program performs time-series analysis. Eos, Trans. Am. Geophys. Union 77. https://doi.org/10.1029/96E000259, 379_379
- Palchan, D., Torfstein, A., 2019. A drop in Sahara dust fluxes records the northern limits of the African Humid Period. Nat. Commun. 10, 3803. https://doi.org/10.1038/ s41467-019-11701-z.
- Palmisano, A., Woodbridge, J., Roberts, C.N., Bevan, A., Fyfe, R., Shennan, S., Cheddadi, R., Greenberg, R., Kaniewski, D., Langgut, D., Leroy, S.A.G., Litt, T., Miebach, A., 2019. Holocene landscape dynamics and long-term population trends in the Levant. Holocene 29, 708–727. https://doi.org/10.1177/0959683619826642.
- Peleg, N., Morin, E., Gvirtzman, H., Enzel, Y., 2012. Rainfall, spring discharge and past human occupancy in the Eastern Mediterranean. Clim. Change 112, 769–789. https://doi.org/10.1007/s10584-011-0232-4.
- Quade, J., Dente, E., Armon, M., Ben Dor, Y., Morin, E., Adam, O., Enzel, Y., 2018. Megalakes in the sahara? A review. Quat. Res. 90, 253–275. https://doi.org/ 10.1017/qua.2018.46.
- Ramsey, C.B., 2008. Deposition models for chronological records. Quat. Sci. Rev. 27, 42–60. https://doi.org/10.1016/j.guascirev.2007.01.019.
- Reimer, P.J., Austin, W.E.N., Bard, E., Bayliss, A., Blackwell, P.G., Bronk Ramsey, C., Butzin, M., Cheng, H., Edwards, R.L., Friedrich, M., Grootes, P.M., Guilderson, T.P., Hajdas, I., Heaton, T.J., Hogg, A.G., Hughen, K.A., Kromer, B., Manning, S.W., Muscheler, R., Palmer, J.G., Pearson, C., van der Plicht, J., Reimer, R.W., Richards, D.A., Scott, E.M., Southon, J.R., Turney, C.S.M., Wacker, L., Adolphi, F., Büntgen, U., Capano, M., Fahrni, S.M., Fogtmann-Schulz, A., Friedrich, R., Köhler, P., Kudsk, S., Miyake, F., Olsen, J., Reinig, F., Sakamoto, M., Sookdeo, A., Talamo, S., 2020. The IntCal20 northern hemisphere radiocarbon age calibration curve (0–55 cal kBP). Radiocarbon 62, 725–757. https://doi.org/10.1017/RDC.2020.41.
- Rodwell, M.J., Hoskins, B.J., 1996. Monsoons and the dynamics of deserts. Q. J. R. Meteorol. Soc. 122, 1385–1404. https://doi.org/10.1256/smsqj.53407.

- Rohling, E.J., Marino, G., Grant, K.M., 2015. Mediterranean climate and oceanography, and the periodic development of anoxic events (sapropels). Earth Sci. Rev. 143, 62–97. https://doi.org/10.1016/j.earscirev.2015.01.008.
- Rossignol-Strick, M., 1987. Rainy periods and bottom water stagnation initiating brine accumulation and metal concentrations: 1. The Late Quaternary. Paleoceanography 2, 333–360. https://doi.org/10.1029/PA002i003p00333.
- Seager, R., Liu, H., Henderson, N., Simpson, I., Kelley, C., Shaw, T., Kushnir, Y., Ting, M., 2014. Causes of increasing aridification of the mediterranean region in response to rising greenhouse gases. J. Clim. 27, 4655–4676. https://doi.org/10.1175/JCLI-D-13-00446.1.
- Shanahan, T.M., McKay, N.P., Hughen, K.A., Overpeck, J.T., Otto-Bliesner, B., Heil, C.W., King, J., Scholz, C.A., Peck, J., 2015. The time-transgressive termination of the african Humid Period. Nat. Geosci. 8, 140–144. https://doi.org/10.1038/ngeo2329.
- Solomina, O.N., Bradley, R.S., Hodgson, D.A., Ivy-Ochs, S., Jomelli, V., Mackintosh, A.N., Nesje, A., Owen, L.A., Wanner, H., Wiles, G.C., Young, N.E., 2015. Holocene glacier fluctuations. Quat. Sci. Rev. 111, 9–34. https://doi.org/10.1016/j. quascirev.2014.11.018.
- Stein, M., Starinsky, A., Katz, A., Goldstein, S.L., Machlus, M., Schramm, A., 1997.
 Strontium isotopic, chemical, and sedimentological evidence for the evolution of Lake Lisan and the Dead Sea. Geochim. Cosmochim. Acta 61, 3975–3992. https://doi.org/10.1016/S0016-7037(97)00191-9.
- Stein, M., Torfstein, A., Gavrieli, I., Yechieli, Y., 2010. Abrupt aridities and salt deposition in the post-glacial Dead Sea and their North Atlantic connection. Quat. Sci. Rev. 29, 567–575. https://doi.org/10.1016/j.quascirev.2009.10.015.
- Stern, O., 2010. Geochemistry, Hydrology and Paleo-Hydrology of Ein Qedem Spring System. Hebrew University of Jerusalem.
- Stuiver, M., Braziunas, T.F., 1989. Atmospheric 14C and century-scale solar oscillations. Nature 338, 405–408. https://doi.org/10.1038/338405a0.
- Torfstein, A., Goldstein, S.L., Kagan, E.J., Stein, M., 2013a. Integrated multi-site U-Th chronology of the last glacial Lake Lisan. Geochim. Cosmochim. Acta 104, 210-231. https://doi.org/10.1016/j.gca.2012.11.003.
- Torfstein, A., Goldstein, S.L., Kushnir, Y., Enzel, Y., Haug, G., Stein, M., 2015. Dead Sea drawdown and monsoonal impacts in the Levant during the last interglacial. Earth Planet Sci. Lett. 412, 235–244. https://doi.org/10.1016/j.epsl.2014.12.013.
- Torfstein, A., Goldstein, S.L., Stein, M., Enzel, Y., 2013b. Impacts of abrupt climate changes in the levant from last glacial Dead Sea levels. Quat. Sci. Rev. 69, 1–7. https://doi.org/10.1016/j.quascirev.2013.02.015.
- Tuel, A., Eltahir, E.A.B., 2020. Why is the mediterranean a climate change hot spot?

 J. Clim. 33, 5829–5843. https://doi.org/10.1175/JCLI-D-19-0910.1.
- Weber, N., Lazar, B., Gavrieli, I., Yechieli, Y., Stein, M., 2021. Gypsum deltas at the Holocene Dead Sea linked to grand solar minima. Geophys. Res. Lett. 48, 1–10. https://doi.org/10.1029/2020GL091034.
- Weinberger, R., Begin, Z.B., Waldmann, N., Gardosh, M., Baer, G., Frumkin, A., Wdowinski, S., 2006. Quaternary rise of the sedom diapir, Dead Sea basin. In: New Frontiers in Dead Sea Paleoenvironmental Research. Geological Society of America. https://doi.org/10.1130/2006.2401(03.
- Xu, H., Goldsmith, Y., Lan, J., Tan, L., Wang, X., Zhou, X., Cheng, J., Lang, Y., Liu, C., 2020. Juxtaposition of western pacific subtropical high on asian summer monsoon shapes subtropical east asian precipitation. Geophys. Res. Lett. 47, 1–10. https://doi. org/10.1029/2019GL084705
- Yechieli, Y., Magaritz, M., Levy, Y., Weber, U., Kafri, U., Woelfli, W., Bonani, G., 1993. Late quaternary geological history of the Dead Sea area. Israel. Quat. Res. 39, 59–67. https://doi.org/10.1006/qres.1993.1007.
- Ziv, B., Saaroni, H., Alpert, P., 2004. The factors governing the summer regime of the eastern Mediterranean. Int. J. Climatol. 24, 1859–1871. https://doi.org/10.1002/ joc.1113.